1992

Pattern formation in a model of an oscillatory Belousov-Zhabotinsky medium

William S. Comstock
The University of Montana

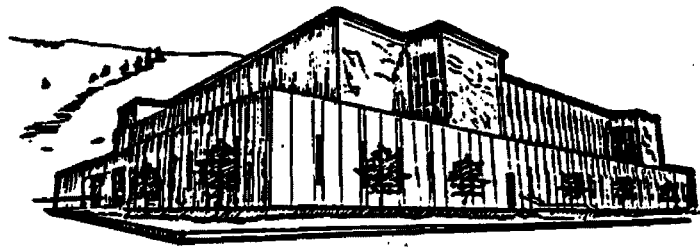# Pattern Formation in a Model of an Oscillatory Belousov-Zhabotinsky Medium

By

William S. Comstock, Jr

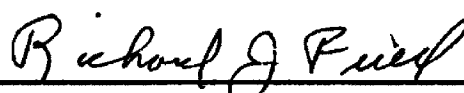B.A. University of Montana, 1984

Presented in partial fulfillment of the requirements

for the degree of

Master of Science
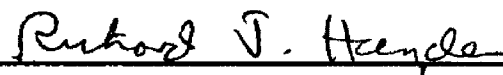
University of Montana

1992

Approved by:

Richard J Field

Co-chairman, Board of Examiners

Richard V. Heindle

Co-chairman, Board of Examiners

C. Murray

Dean, Graduate School

December 15, 1992

Date

UMI Number: EP39171

UMI

Dissertation Publishing

UMI EP39171

ProQuest

Comstock, William S. Jr., M.S., December 1992   Physics

Pattern Formation in a Model of an Oscillatory Belousov-Zhabotinsky Medium (80 pp.)

Directors: Richard J. Field $\varrho \, \partial \, F$ Richard J. Hayden $\mathcal{R} \mathcal{J} \mathcal{H}$

Spontaneous generation of structure in spatially distributed systems may occur when local dynamical elements are coupled by physical transport processes such as conduction or diffusion. Mathematical models of chemical systems whose dynamics are governed by nonlinear kinetic laws play an important role in understanding these phenomena. The Belousov-Zhabotinsky (BZ) reaction is one of the more important in this respect. Solutions in the form of stationary spatial inhomogeneities in the concentrations (patterns) have been found for the Oregonator model of the BZ reaction but their relation to the local dynamics of the chemical system has been unclear. The purpose of this study is to explore the spatial-temporal dynamics of the spatially distributed modified Oregonator model using numerical simulation techniques and to explain the observed behavior using qualitative analysis of the space-dependent nonlinear equations. Of particular interest in this study will be the behavior of the model in an oscillatory regime, when the spatially distributed medium is subjected to finite perturbations.

The theory of waves in reaction-diffusion systems with one dynamical variable will serve as the theoretical foundation for analysis of these phenomena. These results are then extended to characterize wave phenomena in two- and three-variable systems. It is shown that under certain conditions these higher dimensional systems may evolve pattern type solutions by the mechanism of wave stopping and stabilization through self regulation. The characterization of this behavior in terms of the local dynamics of the homogeneous system is emphasized. This will allow a simple analysis of the behavior observed in the model simulations of the space-dependent modified Oregonator.

The results of numerical simulation studies of the spatially distributed modified Oregonator model in a homogenously oscillating state are presented and interpreted in terms of the dynamics of the local subsystem. They show that stable stationary spatial structures do evolve in the space-dependent model by a unique mechanism which is much different from any previously described. The system forms a pulse of excitation each time it undergoes an oscillation. As this occurs regions in the spatial domain are locked into a nonhomogeneous state. Pattern-type structures are left behind as this disturbance propagates across the domain. This observed behavior is interpreted in terms of the stopping of traveling wave fronts and their stabilization through a self-regulatory process. Critical steps in the time sequence of the evolution of a computed stationary structure are characterized in terms of the local dynamics.

Acknowledgements

My appreciation to Dr. Richard J. Field, who has provided not only a great body of research on which to base my work, but continual support, encouragement, and insight throughout my graduate studies.

To Dr. Andrzej Kawczynski, my heartfelt thanks. His great insights provided major elements to the formulation of this research, and his brimming enthusiasm spurred inquires into many fascinating areas. As my mentor and role model for disciplined scientific thought, I'm immensely grateful to him.

Dr. Richard Hayden provided my initiation into the realm of scientific problem-solving. I am appreciative of his ability to foster analytical thinking, and for his encouragement.

My committee members, Dr. Field, Dr. Hayden, and Dr. Uchimoto have been extremely supportive. I wish to thank them for their many valuable suggestions.

For many stimulating and useful discussions, I wish to thank Dr. William Derrick, Dr. Richard Lane and Dr. James Ullrich.

Parts of this research report have been the basis of publications. I wish to gratefully acknowledge my collaborators, Dr. Field and Dr. Kawczynski.

Publications on this research:

1. W.S. Comstock and R.J. Field, Physica D **46** (1990) 139.

2. A.L. Kawczynski, W.S. Comstock and R.J. Field, Physica D **54** (1992) 220.

Table of Contents

iv

List of Tables

v

List of Figures

1. INTRODUCTION

Spatially Distributed Nonlinear Systems

Spatially distributed systems maintained far from equilibrium and governed by non-linear dynamical laws may exhibit self-organizing behavior while dissipating energy [38,59]. Fluid dynamical systems, those systems governed by the nonlinear Navier-Stokes equation, provide many examples [5]. These include the Benard convective cells and Taylor vortices. Spatial structures can arise from a sequence of bifurcations from steady state Benard cells, through oscillatory cells to weak turbulence. Manifestations of these phenomena are apparent in everyday experience, from the form of cloud patterns to the ripples on beach sand. Even the non-uniform distribution of galaxies on a universal scale may be the result of some sort of self-organization due to the highly nonlinear dynamical laws governing the early universe when it was in a much more dense fluid state.

Spontaneous generation of spatiotemporal structure may also appear in chemical and biological systems when local dynamical elements are coupled by physical transport processes such as diffusion or convection. The traveling excitation waves observed in active reacting and diffusing chemical systems are an important example. The planar concentration fronts, spiral waves and target patterns seen in certain chemical reactions probably have biological analogs in such phenomena as signal propagation by repetitive nerve axon impulses [45] and waves of neurological activity in cardiac tissue [61]. A well-studied example is the aggregation of slime mold (Dictyostelium discoideum) amoeba to

1

form colonies [39,58]. The migration of an advantageous gene in a biological population may be modelled as a wave phenomena in a Lotka-Volterra like kinetic system [18]. This is the famous Fisher equation which is a mathematical paradigm for waves in kinetic systems. The propagation of the spruce budworm, a pest to conifers in northern forests, may occur as a wave phenomena and wave models of this system predict methods of control which are now being implemented by forest managers [37].

Spontaneous generation of stationary spatial structures is also possible in chemical and biological systems. It may account for the formation of tissue in the developing embryo (morphogenesis) [33] and the spatial distribution of individuals in a population [40,49]. Again the slime mold has been an important biological laboratory for studying these phenomena. Certain stages in the amoeba aggregation process have been modelled by reaction-diffusion equations [30]. Other workers have found empirical evidence that reaction-diffusion processes may play a role in the formation of the cyclic AMP gradient associated with the differentiation of slime mold spore and stalk cells [3]. The patterning of mammal coats such as the zebra's stripes and leopard's spots may be the result of reaction-diffusion processes forming a chemical pre-pattern in the skin layer which guides the production of pigmentation responsible for the coloring of skin and fur [35].

The chemical theory of morphogenesis attempts to explain differentiation in embryonic tissue in terms of a diffusive instability arising from a steady state reaction-diffusion system. This instability generates a chemical *pre-pattern*, a non-uniform distribution of some chemical species (the *morphogen*), which guides the development of the tissue [33,

62]. Because these morphogens are probably found only as reactive intermediates in extremely low concentrations in the embryonic environment their detection and measurement is very difficult. Thaller and Eichele were the first biochemists to present solid empirical evidence for the existence of a morphogen in embryonic tissue [52]. A good review of the problems associated with the detection of morphogens can be found in Slack [51].

As used in this report *patterns* will refer to stable, stationary, spatially periodic, finite-amplitude inhomogeneities in state variables of the reaction-diffusion equation. They will have an intrinsic length scale which depends only on the internal dynamics and not on the size of the system under consideration. A more descriptive name for them is *stationary periodical (spatial) structures* [28]. Spatial structures of this type are to be distinguished from *standing waves* which may form in vibratory systems due to reflections at the boundaries. The term pattern is sometimes used in the chemical dynamics literature to refer to any sustained spatial inhomogeneity such as traveling pulses and spiral waves. It will be used here only in the more rigorous, historically accurate form which emphasizes the asymptotic stability and stationary nature of the structures.

In 1940 the Russian mathematician Rachevsky proposed a theory to account for biological pattern formation by reaction-diffusion processes [44]. Probably a fatality of the Cold War, his work remained largely unknown in the West until recently. The credit for the discovery of the mathematical theory of morphogenesis is generally given to Alan Turing, a British mathematician who in 1952 investigated this phenomenon using a sim-

ple chemical model of a reaction-diffusion process [53]. He showed that patterns may arise when a stable, spatially homogeneous steady state loses stability to infinitesimal perturbations of nonzero wavenumber. This is also known as a diffusive instability. Although no unequivocal empirical evidence for the existence of such pattern formation mechanisms in chemical (or biological) systems has been found in the forty years since Turing's original paper, the subject has continued to generate fascination and to receive considerable theoretical and experimental attention. This is partially due to its implications for explaining the biological differentiation process in embryology in terms of basic biochemical principles. Much of this effort has concentrated on the application of bifurcation techniques to analysis of the effect of diffusion on the stability of homogeneous steady states close to a Hopf bifurcation [38]. This type of analysis involves small-amplitude patterns and emphasizes the loss of stability of a far-from-equilibrium steady state which is a continuation of the state of chemical equilibrium. Patterns have been found using these techniques in many chemical models [38,54] when there is an asymmetry in diffusion coefficient values.

Patterns also may arise when a spatially homogeneous system far from any bifurcation is subject to a large-amplitude disturbance [2,22,23,29]. The system in this case must be at least excitable in the sense that such a perturbation may cause the system to jump to some qualitatively different state. The decay of such a disturbance to spatial homogeneity if it fails to exceed some threshold or its evolution to a pattern can be investigated using both the theory of nonlinear reaction-diffusion equations and numerical

techniques [22,23,47]. The form and evolution of patterns is determined by both the properties of the internal dynamics of the system and the characteristics of the disturbance. These patterns may coexist with others of a different form or with spatially homogeneous states.

Mention should be made of another approach to the problem of biological pattern formation. The mechanicochemical approach to pattern formation in biological systems [37] emphasizes the role of mechanical forces in development. This theory addresses the problem of the extreme difficulty of measuring the chemical morphogens postulated by the reaction-diffusion theory of embryonic development. Its models are mathematically quite complex but tend to deal with quantities such as cell densities, forces, and tissue deformation which are experimentally observable biological properties rather than the more abstract reaction-diffusion morphogenetic models. Pattern formation processes which occur during development probably result from a combination of chemical morphogenetic and mechanical processes.

Chemical Models for Pattern Formation

Chemical models play an important role in the study of spatiotemporal structures in nonlinear dynamical systems. They provide experimental evidence for the existence of such structures in nature. Historically many of the important nonlinear phenomena were first systematically observed in chemical systems. In the biological context it is clear that the actual mechanisms of organization are rooted in biophysical and biochemical interactions which must be reducible to basic physical and chemical principles. This reduction

is extremely difficult and has only been performed in a few simple cases but must remain an ultimate goal for understanding life processes. Chemical systems may also serve as important analogies for processes in living organisms. Though the detailed chemical mechanistic processes may often differ from those in biological systems, the study of chemical systems may alert us to the existence or importance of macroscopic phenomena which transcends these mechanistic details.

Certain chemical models have been of particular interest in this respect. They include the Brusselator [38], various models of the Belousov-Zhabotinsky (BZ) reaction [13], models of the Gray-Scott system [60], abstract enzymatic-substrate inhibition systems [28,35] and the models of the chorite-iodide system [6]. Many of these models are of the activator-inhibitor type which display a wide range of interesting dynamical behavior and can be described by relatively simple mathematical models.

The Oregonator model of the BZ reaction is particularly significant in this respect. Though the chemistry of the BZ is unrelated to any biological systems it provides many profound analogies to dynamical phenomena observed in biological systems. Multiple steady states, oscillations, chaos and propagating spatial structures have been observed both experimentally in the BZ and in numerical simulation studies based on the Oregonator model. Solutions in the form of patterns have be found in numerical experiments with BZ models [2,20,47]. These have demonstrated the theoretical possibility of pattern formation in this reaction and resolved the long-standing controversy over whether such patterns resulted from hydrodynamic effects rather than internal dynamics. However,

that work has left many questions open concerning the mechanisms of pattern formation and their realization in experimental systems.

Statement of the Problem

This report will address two important problems concerning pattern formation in the Oregonator model of the BZ reaction. It will utilize numerical simulations of the space-dependent version of the model in conjunction with the techniques of nonlinear analysis of wave front propagation in reaction-diffusion systems to examine these problems.

The first problem is to explain the pattern formation mechanism in the BZ model. Previous work on pattern formation in the Oregonator model characterized the necessary conditions for the existence of stationary solutions [2]. However, these conditions were not clearly related to either known properties of systems undergoing Turing bifurcations or the theory of propagating fronts in excitable systems. In another work [19] an elaborate construction involving trigonometric series was used to derive sufficient conditions for the existence of stationary solutions for the Oregonator model. Unfortunately, the solutions were unstable when subjected to small perturbations. The failure to characterize these conditions in terms of the known properties of reacting and diffusing systems undergoing wave propagation or diffusive destabilization probably led to the lack of recognition of the inherent instability of those solutions. The mechanism of the actual evolution of the patterns was not characterized in either of these cases.

Rovinsky [47] presents theoretical and numerical-experimental evidence for the existence of both a classical Turing-type instability and large amplitude stationary wave

fronts in a two variable Fe catalyzed model of the BZ reaction. Since that model and the Oregonator both describe the same chemical system there is some hope that such solutions may be found for the Oregonator. However, such instabilities have not yet been found in the Oregonator even though the model is an activator-inhibitor type system and exhibits the general conditions such as autocatalysis and negative feedback necessary for such behavior.

Any analysis of the results of numerical simulation of the Oregonator model of the BZ reaction should be based on the well-established theory for the wave dynamics of nonlinear reaction-diffusion systems. An attempt will be made to determine the conditions for pattern formation in terms of the local dynamics of the much simpler spatially homogeneous system and characterize the evolution of patterns in terms of known properties of propagating waves in reaction-diffusion systems. This characterization should again be based on the dynamics of the local system.

The second problem which will be addressed here is that of pattern formation with near-equal diffusion coefficients. As already pointed out, previous research has demonstrated the existence of stationary spatially non-homogeneous solutions for the reaction-diffusion equations arising from the Oregonator [2]. However, patterns were found only when the diffusion coefficient of the catalyst species was much larger than those of the other reactive intermediates. This observation agrees with the theory of diffusive instabilities in activator-inhibitor systems which require that the inhibitor diffuse much more rapidly than the activator [36]. In the case of the BZ reaction the metal ion catalyst spe-

cies acts as an inhibitor because it inhibits the growth of $HBrO_2$ (the "activator") by producing Br^-. Unfortunately, it is known that in the actual chemical system the catalyst species actually diffuses much more slowly than the other reactive intermediates. This fact would seem to rule out the possibility of pattern formation in the BZ reaction resulting from the Turing-type diffusive instabilities. However it has been pointed out that stationary spatial structures may evolve in chemical systems by other mechanisms -- in particular the large amplitude perturbation of systems with excitable kinetics [47]. It should also be noted that patterns arising from diffusive instabilities may occur in activator-inhibitor type systems with equal diffusion coefficients when an external concentration gradient is imposed. In that case the gradient itself is sufficient to destabilize the system without requiring the asymmetry of the rate of diffusion of the intermediate species.

Overview of this Report

The evolution of patterns from an homogeneous oscillatory state subject to a finite perturbation is reported here. That evolution is described in terms of the properties of propagating wave fronts in nonlinear reaction-diffusion systems. Conditions for the existence of traveling front solutions and the dependence of their velocity on the systems' local dynamics play a crucial role in this development. Appropriate conditions are formulated for application of these considerations to two and then three-variable systems. These ideas then are used to interpret the results of numerical simulation of the behavior of a modified Oregonator model of the Belousov-Zhabotinsky reaction. The results will

show that stable stationary spatial structures may evolve by a mechanism much different from any previously described and that this evolution and the properties of these structures can be characterized in terms of the local dynamics of the system.

First the chemistry of the BZ reaction will be reviewed and models of its kinetics discussed. The modified Oregonator model will then be presented. The theory of wave phenomena in one dimensional reaction-diffusion systems will then be described in some detail and an example system analyzed. These results are then extended to higher dimensional systems leading to the postulation of a conjecture which will help characterize the evolution of patterns in the modified Oregonator. A detailed description of the evolution observed in a numerical simulation of the homogeneously oscillating model will then be given. That analysis will highlight the critical points in the evolution to the final stationary structure. There follows a short discussion of the implication of these results and suggestions for additional research in this area. Finally, the appendix contains brief descriptions of the software used in this project and information on its availability.

2. MODELS FOR THE KINETICS OF THE BELOUSOV-ZHABOTINSKY REACTION

FKN - The chemistry of the BZ

The BZ reaction is in the most simple terms the monotonic oxidation of an organic substrate (usually malonic acid) by bromate ion in a strong acidic medium. This transformation is catalyzed by a metal ion (typically Ferroin or Cerium) which has two oxidation states separated by a single electron. The overall reaction scheme can be expressed as

$$2H^+ + 2BrO_3^- + 3CH_2(COOH)_2 \rightarrow 2BrCH(COOH)_2 + 4H_2O + 2CO_2.$$

This reaction thermodynamically drives the non-monotonic behavior of the intermediate species $HBrO_2$, Br^-, $HOBr$, BrO_3^- and the catalyst. Examples of this behavior observed in spatially homogeneous systems include oscillations, excitability, bi- and tri-stability, hysteresis (the coexistence of oscillatory and steady states) and deterministic chaos [13]. Traveling excitation fronts have been observed experimentally [63] in un-stirred systems. A model chemical mechanism which describes much of this behavior has been reduced to a series of 18 elementary reactions by Field, Körös and Noyes (FKN) [9]. That mechanism successfully describes much of the known experimentally observed dynamical behavior of the BZ. It is based on the existence of two non-interacting processes (A and B) which are coupled by a third process (C) which switches control between the competing processes A and B. Bromide ion is the critical intermedi-

11

ate in this interaction whose concentration determines whether Process A (high bromide — the catalyst is in a reduced state) or Process B (low bromide — the catalyst is in its oxidized state) is dominant. The switching between the reaction processes occurs in an essentially oscillatory manner since Process A consumes bromide ion until a critical level is reached at which time Process B takes control. Process B then indirectly produces bromide ions until sufficient quantity has accumulated and control returned to Process A.

The Oregonator

While the FKN mechanism provides a detailed understanding of much of the chemistry of the BZ its size makes it very difficult to use in mathematical modelling. The Oregonator model of the BZ reaction is an abstract mechanism which considerably simplifies the mathematical analysis of the FKN and qualitatively reproduces much of the dynamical behavior of the Belousov-Zhabotinsky reaction. It consists of the following five reaction steps along with their rate constants [10]:

$$
\begin{array}{lll}
A + Y \rightarrow X + P & (M1) & k_{M_1} = 2.5[H^+]^2\,M^{-3}s^{-1} \\
X + Y \rightarrow P + P & (M2) & k_{M_2} = 3.0 \times 10^6\,[H^+]\,M^{-2}s^{-1} \\
A + X \rightarrow 2X + Z & (M3) & k_{M_3} = 40\,[H^+]\,M^{-2}s^{-1} \\
X + X \rightarrow A + P & (M4) & k_{M_4} = 3.0 \times 10^3\,M^{-1}\,s^{-1} \\
Z \rightarrow f\,Y & (M5) & k_{M_5} = 0.1\,s^{-1}
\end{array}
$$
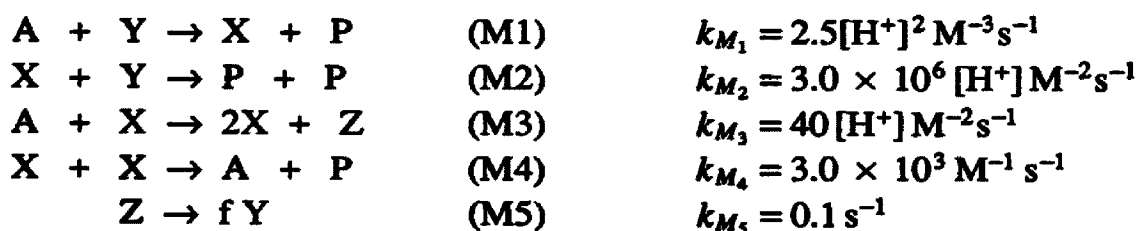
The model variables are related to the experimentally observable chemical species by the associations

$$X \equiv [HBrO_2], \qquad Y \equiv [Br^-], \qquad Z \equiv 2[Ce(IV)],$$

$$A \equiv [BrO_3^-] \text{ and } \qquad P \equiv [HOBr].$$
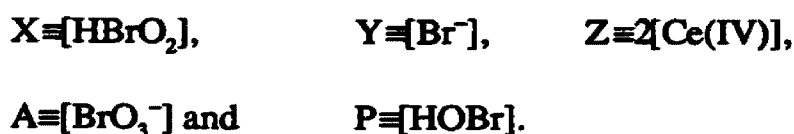
The skeleton of the FKN can be recognized in the Oregonator by identifying steps (M1) and (M2) as Process A, (M3) and (M4) as Process B and (M5) as representing the chemistry of Process C. The rate constants for steps (M1) through (M4) are from [8] and will be taken as fixed constants throughout this work. Because step (M5) of the Oregonator represents an overall stoichiometry rather than a simple reaction step [13] its rate constant and stoichiometric factor f are generally considered as expendable parameters. The values [H$^+$]=0.8 M and A=0.06 M will be treated as constants in the calculations reported here.

Modification of the Oregonator - ODEs

Before application of the law of mass action to the Oregonator reaction scheme, a modification suggested by Tyson [54] should be made. It was suggested there that in contrast to the classical Oregonator where the rate of reduction of BrO$_3^-$ by Ce(III) in step (M3) is simply proportional to bromate concentration that it is also linearly proportional to the Ce(III) concentration. This assumption increases the robustness of the model since the concentration of Ce(IV) can never exceed the total catalyst concentration in the reaction vessel. That is, C_{total}=[Ce(III)]+[Ce(IV)] is a conserved quantity in the reaction model. This modification probably also improves quantitative agreement with experiment and adds a new parameter to the model which has a direct connection with experimental procedures. Using this assumption while applying the law of mass action to get the corresponding rate laws yields the reaction dynamics for this modification of

the Oregonator model in the form of a system of nonlinear ordinary differential equations. Their form after dimensional analysis is given by

$$\frac{dx}{dt} = s\left[y - xy + x\left(1 - \frac{z}{c}\right) - qx^2\right] \equiv f(x,y,z)$$

$$\frac{dy}{dt} = \frac{1}{s}\left[-y - xy + fz\right] \equiv g(x,y,z) \tag{1}$$

$$\frac{dz}{dt} = w\left[x\left(1 - \frac{z}{c}\right) - z\right] \equiv h(x,z).$$

This system of equations is scaled according to [10]. The scaled variables are related to the Oregonator model variables by

$$X = \frac{k_{M_1}A}{k_{M_2}}x, \qquad\qquad Y = \frac{k_{M_3}A}{k_{M_2}}y, \qquad\qquad Z = \frac{k_{M_1}k_{M_3}A^2}{k_{M_2}k_{M_5}}z,$$

$$C_{total} = \frac{k_{M_1}k_{M_3}A^2}{k_{M_2}k_{M_5}}c, \qquad\qquad T = \frac{t}{A\sqrt{k_{M_1}k_{M_3}}},$$

$$s = \sqrt{\frac{k_{M_3}}{k_{M_1}}}, \qquad\qquad q = \frac{2k_{M_1}k_{M_4}}{k_{M_2}k_{M_3}}, \qquad\qquad w = \frac{k_{M_5}}{A\sqrt{k_{M_1}k_{M_3}}}.$$

The variables x, y, z and c are the non-dimensionalized values of the concentrations X, Y, Z, and C_{total}, and t is the scaled time. The constant parameters s, q and w are also dimensionless and are related to rate constant values [8]. The chemical model of the BZ reaction whose dynamics are governed by the system of equations (1) will be referred to in this report as the *modified Oregonator*. Numerical simulations of the spatial-temporal evolution of this system are described in detail later in this report.

Other models

Two other mathematical models of the BZ reaction are worthy of mention here. Each of them has seen extensive use in numerical and analytical studies of spatial structures in the BZ. Tyson and Fife [55] used a two variable model with Ferroin catalyst to analyze spiral waves in the BZ medium. That model is essentially a reduction of the Oregonator based on solving the homogeneous equation governing Br^- production for the y variable in terms of x and z. This yields a particularly simple mathematical system which has been widely used in the study of complex scroll patterns and their manifestation as plane and spiral waves. Stationary spatial structures have not yet been explored using that model.

Rovinsky and Zhabotinsky [46] have developed a slightly more complex model system which attempts to account explicitly for the experimentally observed differences in oscillatory behavior in the Ferroin from that of the Cerium catalyzed system. Plane waves, spiral waves and patterns arising from diffusive instability have been found in the analysis of that system.

3. THEORY - FRONT SOLUTIONS TO REACTION-DIFFUSION EQUATIONS

General Considerations

The behavior of spatially distributed dynamical systems in which mass transport occurs only by diffusion can be characterized by the *reaction-diffusion* equation,

$$U_t - D\nabla^2 U = F(U, \Lambda). \tag{2}$$

Here U is a vector of dynamical variables $U=(u_1, u_2, \ldots, u_n)^T$ which characterizes the state of the system at each point in time and space within the problem domain. The subscript indicates differentiation with respect to the time variable t and ∇^2 is the Laplacian operator in the given problem geometry. D is a matrix of diffusion coefficients which characterizes the "strength" of the diffusive coupling of the local dynamical elements. The vector F is a set of nonlinear functions $F=(f_1, f_2, \ldots, f_n)^T$ describing the internal dynamics of U. These are the laws governing the interactions of the u_i. The functional notation for F indicates that each f_j may depend on all the u_i as well as a set of constant parameters $\Lambda=(\lambda_1, \lambda_2, \ldots, \lambda_m)^T$. Changes in the parameters, λ_i, may produce qualitative changes in the behavior of the system; Λ is a vector of bifurcation parameters. The left hand side of Equation (2) is a linear parabolic partial differential operator for U. A problem of this type is sometimes referred to as *quasilinear* [1] to emphasize the linearity of

16

the differential operator itself as opposed to the nonlinear elements of the dynamics F.

Note that if the right hand side is trivial Equation (2) reduces to the classical *diffusion* equation for which there is a well developed body of knowledge [26]. The *local* or *spatially homogenous* system for the reaction-diffusion equation is defined as

$$U_t = F(U, \Lambda).$$

This system of ordinary differential equations for U will be useful in the analysis and characterization of the behavior of the full reaction-diffusion equation.

Equation (2) is usually solved as an initial-value problem in an infinite domain or as an initial-boundary value problem in a spatially bounded domain. The existence and uniqueness of asymptotic solutions are assured by the smoothness properties of F, but the theory of such equations is far from complete. In particular, the evolution to and the properties of asymptotic solutions as well as the coexistence of these solutions for different initial conditions are open questions. In the remainder of this report the following conditions will be assumed to hold for Equation (2). The spatial domain will be constrained to that of one dimensional linear geometry with spatial coordinate *r*. The medium in which the system is diffusing is homogenous and isotropic with no drift effects. This assumption will assure that there are no cross coupling terms in the diffusion matrix -- all nonzero diffusion terms will be found on the diagonal. In addition F must be continuously differentiable for the problem to be well posed and will have no explicit dependence on the space or time variables. Note that in most kinetic-type problems the components of F will be polynomial in the state variables.

The Scalar Problem

The properties of solutions of Equation (2) are known only for trivial or very simple cases. Rigorous analytical results exist only for systems of one dynamical variable where the system may be written as

$$u_t - u_{rr} = f(u, \lambda).\qquad(3)$$

The analysis of this equation will be worked out in some detail in order to lay the groundwork for later development. Note that the one-dimensional diffusion matrix can always be taken as unity in this case by rescaling the spatial coordinate. Solutions of Equation (3) will be sought in the form of constant velocity traveling waves. (Note that in the case being considered here a non-dispersive medium is assumed). That is, u must have the functional form $u(r,t)=U(\xi)$ with $\xi=r - ct$ where c is the wave velocity and $U(\xi)$ must monotonically approach distinct limits as $\xi \rightarrow \pm\infty$. Since the derivatives in Equation (3) must vanish as $r \rightarrow \infty$ these limits must be zeros of the local dynamics f. Substituting $U(\xi)$ into Equation (3) and performing the differentiations yields a second order ordinary differential equation for U,

$$U'' + cU' + f(U,\lambda) = 0.\qquad(4)$$

In this equation primes denote differentiation with respect to the wave variable ξ.

This system can be analyzed in the phase plane by using the standard reduction to first

order,

$$\frac{dU}{d\xi} = V,$$

$$\frac{dV}{d\xi} = -cV - f(U, \lambda).$$

(5)

Traveling wave solutions of Equation (3) can then be represented as orbits connecting

critical points in the (U, V) phase plane for equations (5). The existence and uniqueness

of such trajectories will depend on the type of critical points involved. Fife [14] and Fife

and McLeod [15] have carried out a rigorous classification of the critical points of

Equation (5) and shown that there are just two cases which give rise to traveling wave

solutions for Equation (3). These are the *saddle - saddle* and *saddle - node* connections

or orbits in the phase plane named for the type of critical points involved. The case of

interest here is the saddle - saddle type transition where $f'(u_1)<0$, $f'(u_3)<0$ and f has a

single zero, u_2 in (u_1, u_3) where u_1 and u_3 are also zeros of f. In that case an explicit ex-

pression for the wave velocity may be obtained from Equation (4) by multiplying it by U'

and integrating from $-\infty$ to $+\infty$. Integrating by parts and applying the boundary condi-

tions $U(-\infty)=u_1$ and $U(+\infty)=u_3$ yields

$$c \int_{-\infty}^{+\infty} [U']^2 d\xi = -\int_{u_1}^{u_3} f(u, \lambda) \, du.$$

(6)

This result says that since the integral on the left is always positive the wave velocity, c, will be proportional, with opposite sign, to the area bounded by $f(u)$ on the interval enclosing the two attracting zeros of $f(u_1,u_3)$. The direction of front propagation will then be determined by the sign of the integral on the right. This formula has important consequences when the dynamics f depends continuously on the parameter λ. In that case the propagation speed and direction of the front can be controlled by varying λ [28]. A model of a chemical pulsar [29] has been constructed in which a variable corresponding to λ oscillates in such a way that a traveling wave periodically changes direction.

Kanel [27], working in the theory of combustion, proved that under very general conditions a solution converges to a traveling front for the initial value problem of Equation (3) if

1) $f(u)$ has three distinct zeros, $u_1 < u_2 < u_3$, with u_1 and u_3 linearly stable in the local system for Equation (3) and u_2 unstable in the local system (Figure 1a), and

2) one part of the initial distribution of u is in the basin of attraction of u_1 and the remainder is in the basin of u_3.

The asymptotic form of the traveling front connecting these two zeros is shown in Figure 1b. Equation (3) also has a solution close to a traveling front on a bounded do-
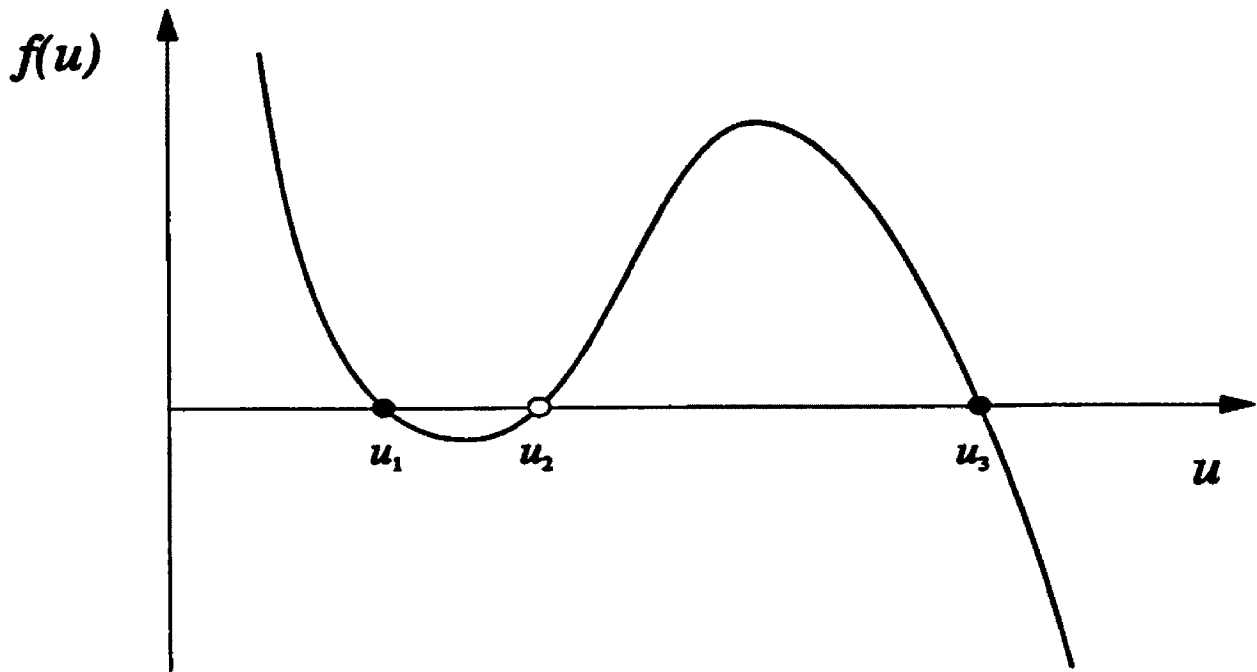
(a)
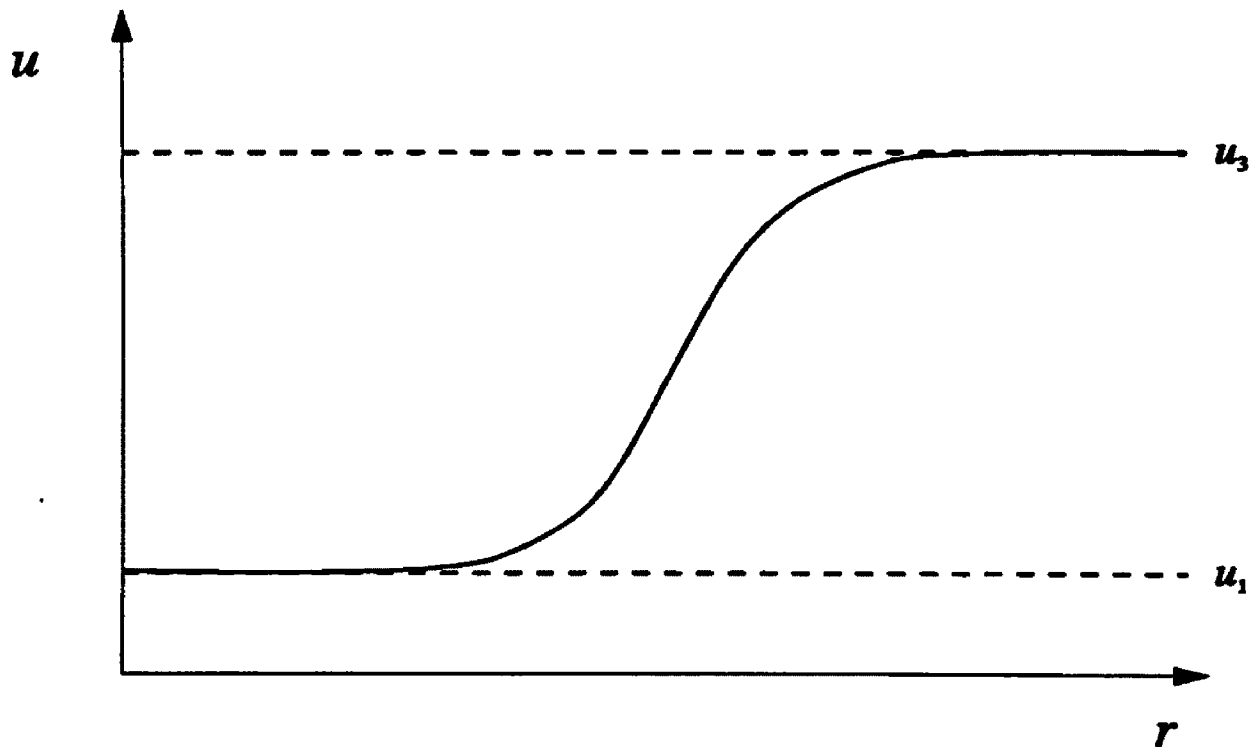
(b)

Figure 1. a) The zeros of $f(u)$ in a general case where the Kanel theorem is applicable. The zeros u_1 and u_3 are attracting while u_2 is repelling. b) Typical example of a front in this system.

main with the initial conditions described above and with no-flux boundary conditions if the jump connecting the basins of attraction is sufficiently far from the boundary.

Example of a one dimensional system satisfying the Kanel theorem. As an illustration of the above theorem and as an initial test of the numerical techniques used later in this report consider the one dimensional reaction-diffusion system, Equation (3), with local dynamics in the form of a cubic [29,38]:

$$f(u, \lambda) = u(u - \lambda)(1 - u), \qquad 0 < \lambda < 1. \tag{7}$$

This simple cubic system has three zeros on [0,1] and satisfies the conditions for the application of Kanel's theorem. It illustrates some of the important principles which will be used later in the analysis of waves in the BZ model. A similar type of dynamics appears in the reduced Nagamo equation which is a simplified form of the FitzHugh-Nagamo model for nerve action potentials. A similar equation has also been used in a model of the *chemical pulsar* [29]. Figure 2 shows the graph of f for several values of the parameter λ. The phase plane orbits from Equation (5) with these dynamics are given by

$$\frac{dU}{dz} = V,$$

$$\frac{dV}{dz} = -cV - U(U - \lambda)(1 - U). \tag{8}$$
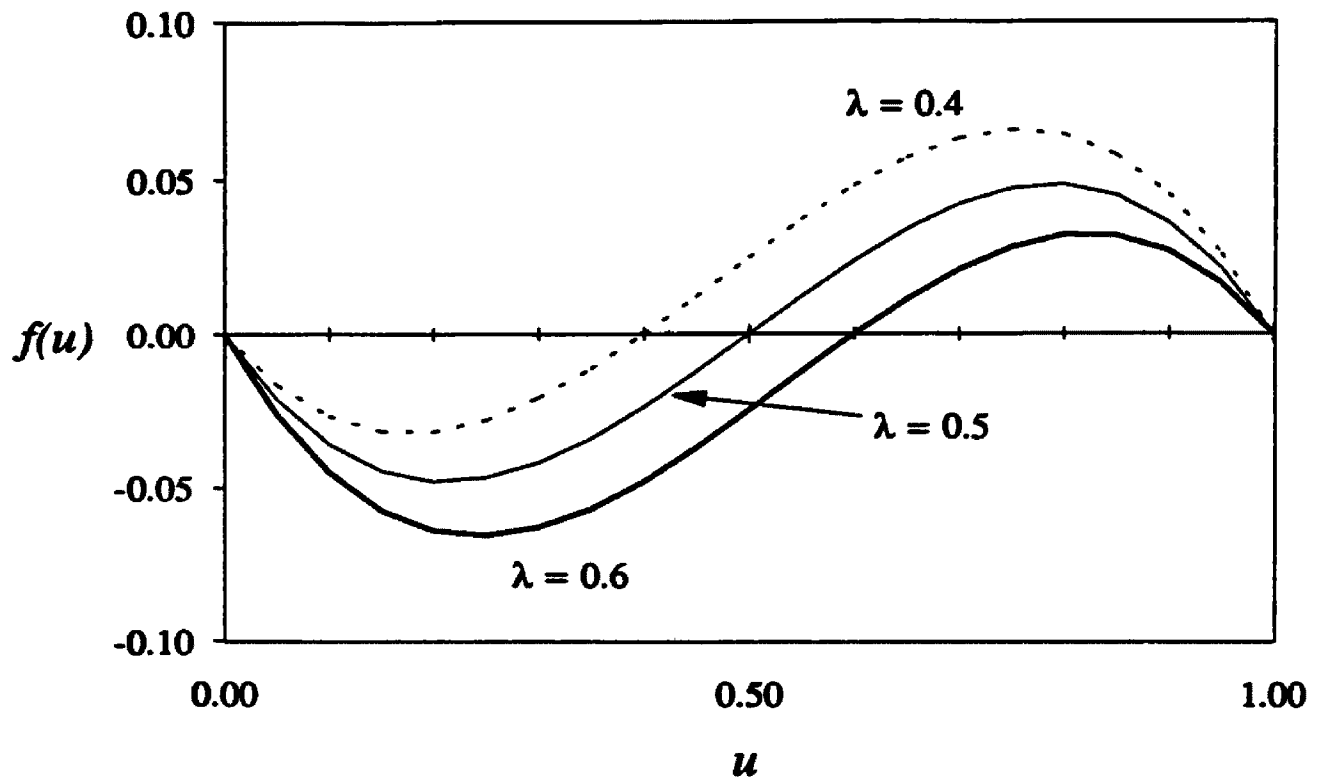
Figure 2. The function $f(u)$ for cubic dynamics (Equation 7) for several values of the parameter λ. Inspection of the graph shows that the zeros, $u=0$ and $u=1$, of f are linearly stable ($f'(0)$, $f'(1)<0$) with the interior zero, $u=\lambda$, unstable ($f'(\lambda)>0$). The area bounded by the $\lambda=0.4$ curve is positive so the wave velocity from Equation (6) will be negative. In a similar manner the area bounded by the $\lambda=0.6$ curve is negative and the velocity positive so the wave will move to the right. The stopping value for the wave is $\lambda=0.5$ since the integral in Equation (6) vanishes.

This system has critical points at (0,0), $(\lambda,0)$, and (1,0), corresponding to the zeros of

$f(u)$ in Equation (7). Linear stability analysis shows that the type of critical points will

depend on the value of the bifurcation parameter λ. In all cases for $0<\lambda<1$ the system sa-

tisfies the conditions for the application of Kanel's theorem. Figures 3 and 4 show phase

plane trajectories of waves in this system for $c<0$ and $c>0$ respectively. There is a unique

value of c corresponding to a particular λ for which the connection between the
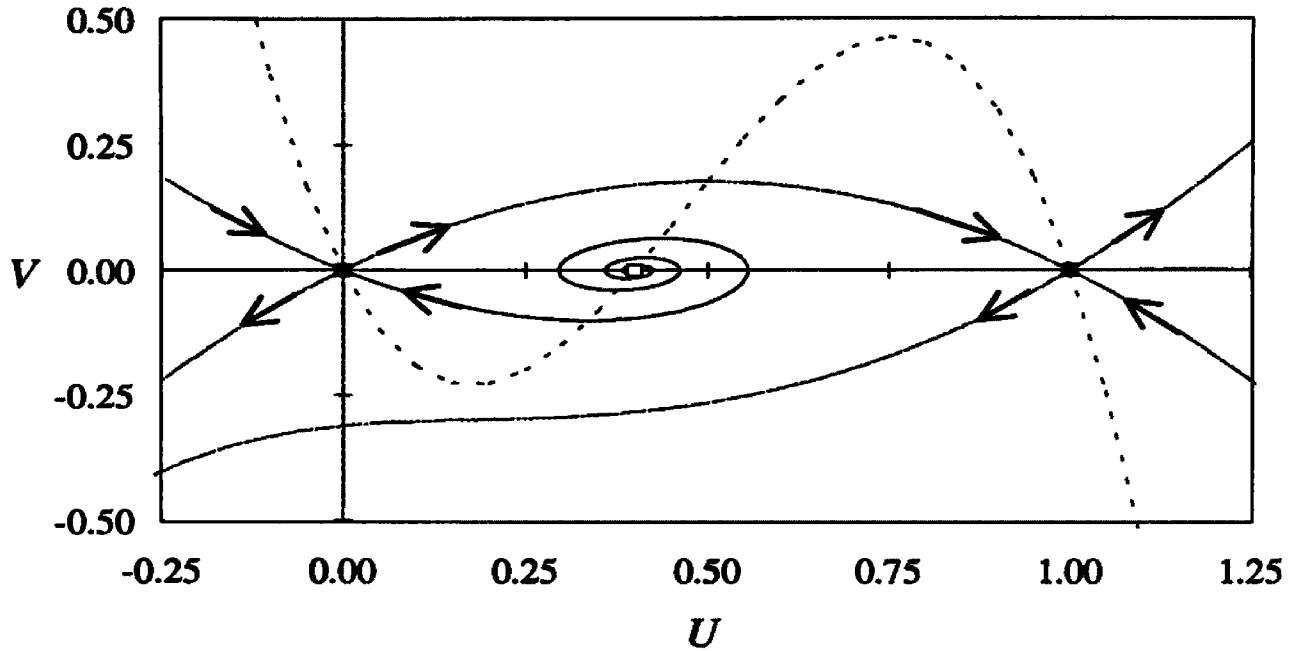
Figure 3. Phase plane orbits for waves in the cubic system for $c < 0$. In this case the singular point $u=\lambda$ is an unstable node. The wave is the trajectory leaving the saddle at (0,0) and entering the saddle at (1,0).
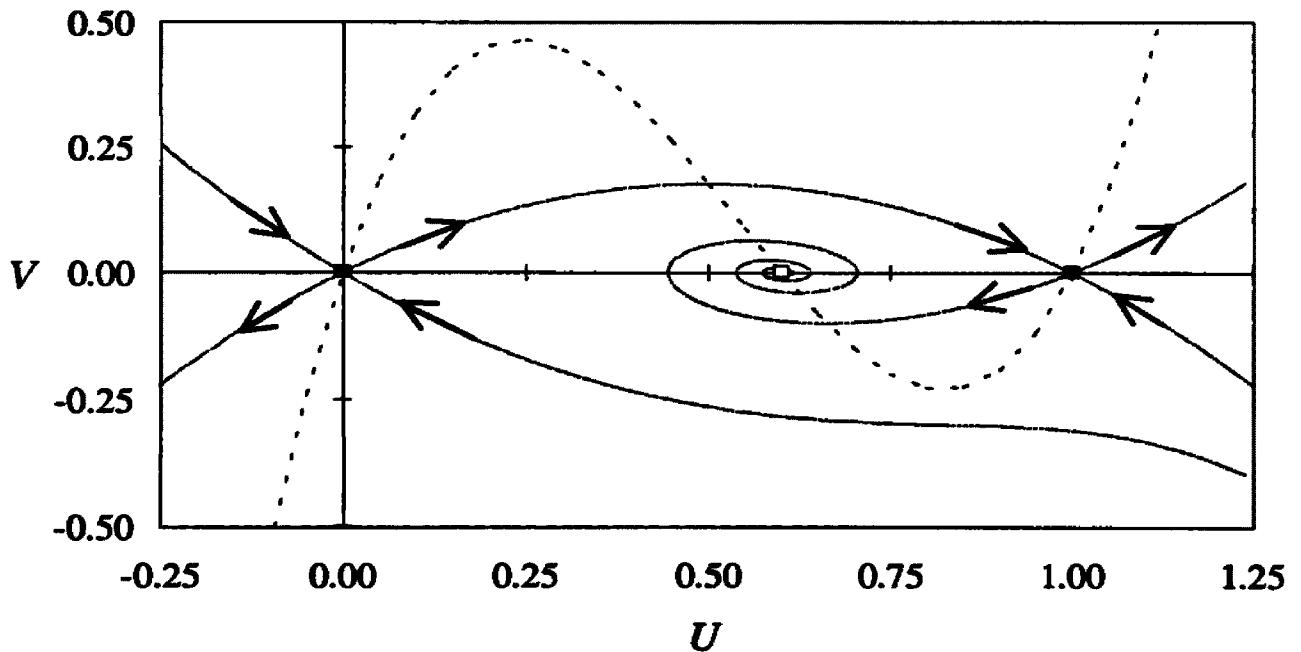
Figure 4. Phase plane orbits for a wave in the cubic system for $c > 0$. Again the wave is the orbit connecting the (0,0) and (1,0) saddles. The point $u=\lambda$ is a stable focus.

saddles at (0,0) and (1,0) exists. The system Equation (8) doesn't provide a practical method to obtain actual solutions for the saddle - saddle type wave dynamics since both λ and c must be known before integration of that system is possible. However, an analytical solution to Equation (3) with cubic dynamics has been worked out [29] and is given by

$$U(\xi) = \frac{1}{1 + e^{-\beta\xi}},$$

with

$$\beta = \frac{1}{\sqrt{2}} \quad \text{and} \quad c = \frac{1}{\sqrt{2}}(1 - 2\lambda).$$

This gives an explicit relation between c and λ which may be used in the system of Equation (8). The reaction-diffusion system, Equation (3), with cubic dynamics, Equation (7), can also be numerically integrated. Solutions obtained in this manner can then be compared to the analytical expression above. Figure 5 shows front solutions obtained by both numerical integration and evaluation of the analytical solution. It shows good qualitative agreement in the shape and motion of the wave front solutions for the cubic. The dependence of wave velocities on λ can also be determined both analytically and numerically. Figure 6 shows numerically computed wave velocities for this system along with those obtained using the analytic expression for c. Note that in the figure the numerically computed velocities show a range for λ where c is close to zero. This is characteristic of numerical calculations for waves with small velocities. Finer spatial grids will shorten this interval but cannot eliminate it completely.
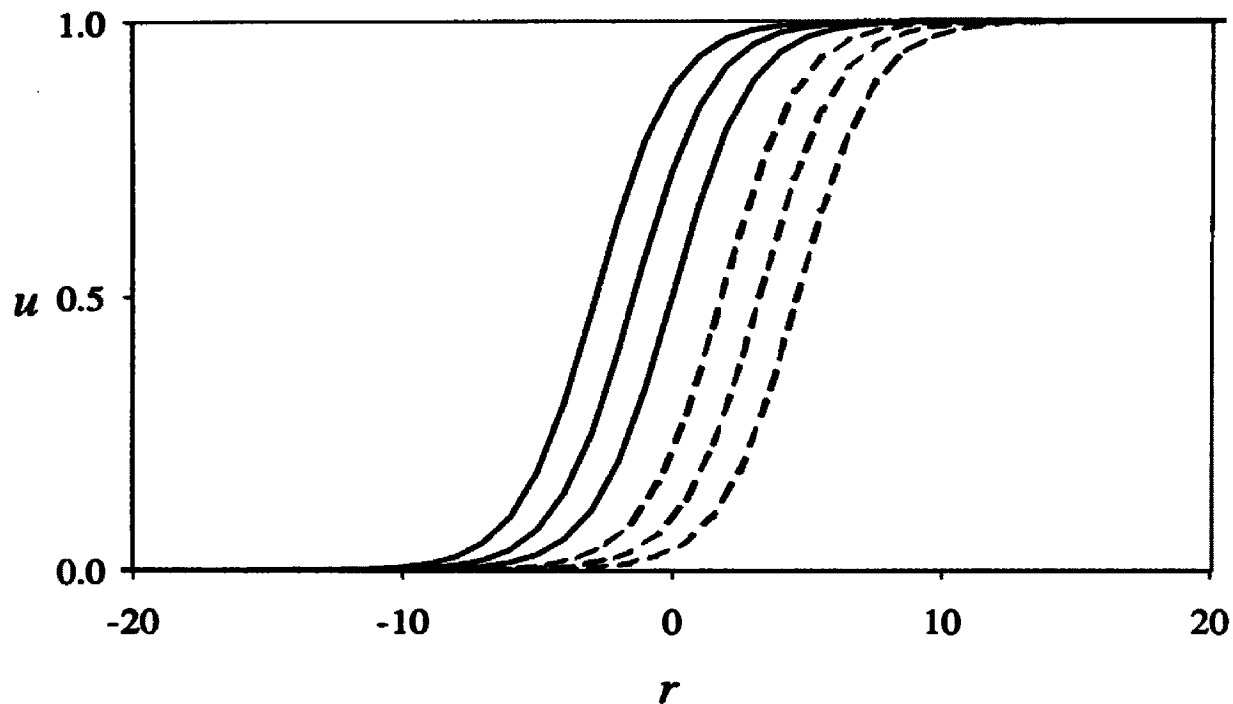
Figure 5. Wave front profiles from numerically (dashed lines) and analytically (solid lines) obtained solutions for the reaction-diffusion system with cubic dynamics.
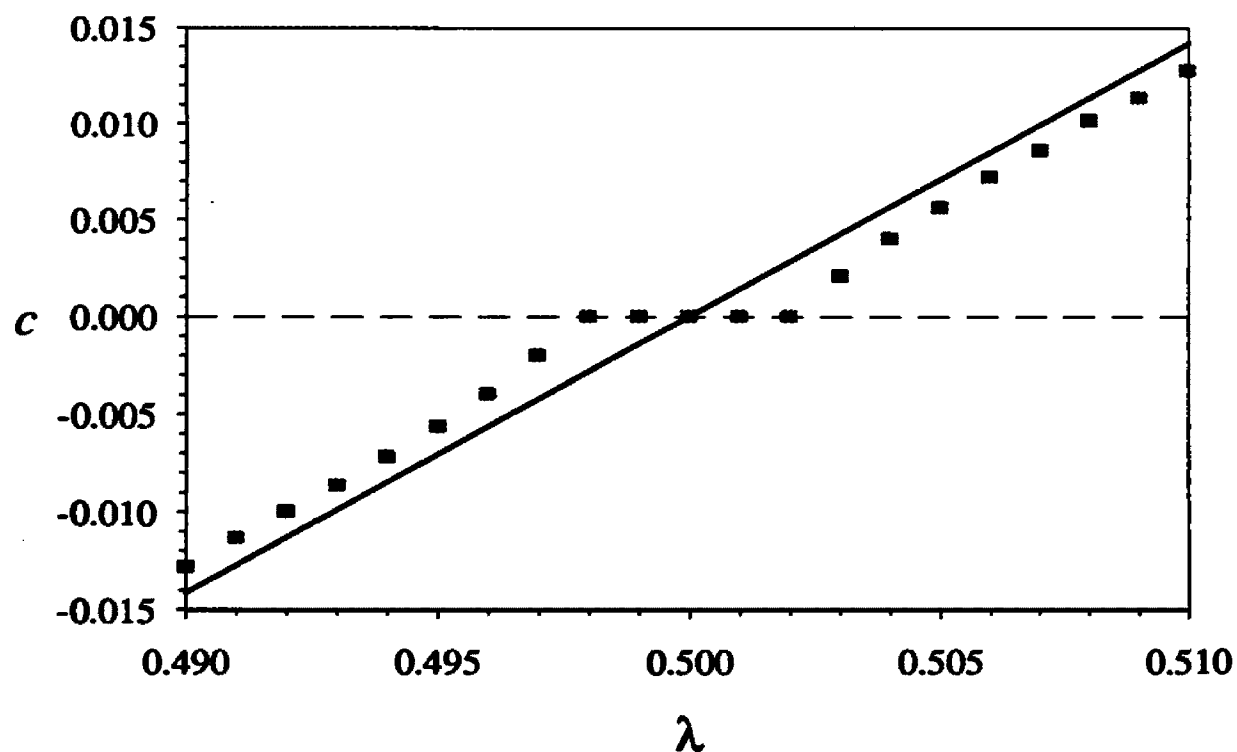
Figure 6. Wave velocities for the cubic system from numerical integration (squares) and the analytical solution (solid line).

The other general type of dynamics for Equation (3) which can give rise to traveling fronts are the *saddle - node* type connections. These solutions are also of interest in the study of chemical and biological systems. Equations of that type were first rigorously analyzed by Kolmogorov, Petrovskii, and Piscunov [32] and proposed as a model of gene migration in a population at the same time by Fisher [19]. Field and Noyes [12] developed a simplified model of front propagation in the BZ which involves only $HBrO_2$ and reduces to a *saddle - node* type system similar to the Fisher equation when their equation was appropriately scaled. An analytical expression for a bound on the wave velocity can be computed for this case [15,32] and has been shown to be in close agreement with experimentally observed values [12,33]. Saul & Showalter [49] used a system with saddle - node dynamics in the derivation of an analytical solution for a model of the iodate-arsenous acid reaction.

Application to Two-Variable Systems

Traveling fronts may also exist in systems of two or more independent variables [60,15]. No rigorous general analytical theory is known for this case. However, in analogy to one-variable systems, fronts may evolve from appropriate initial conditions when a pair of attracting nodes bracket a saddle point in the phase space for the local system. The behavior and properties of such systems can sometimes be characterized in a qualitative way and this characterization supported by numerical simulations of model systems [43,56,35].

Consider a two-dimensional reaction-diffusion system which depends continuously on some parameter λ:

$$\frac{\partial x}{\partial t} - D_x \frac{\partial^2 x}{\partial r^2} = \frac{1}{\varepsilon} f(x, y, \lambda)$$

$$\frac{\partial y}{\partial t} - D_y \frac{\partial^2 y}{\partial r^2} = g(x, y, \lambda)$$

(9)

Assume that the dynamics of x is fast as compared to that of y ($\varepsilon \ll 1$) and that the x-y nullclines obtained from the local dynamics $f(x,y,z)$ and $g(x,y,z)$ have three intersections (singular points) for $\lambda \in (\lambda_1, \lambda_2)$ and that two of these singular points, $((x_1, y_1)$ and $(x_3, y_3))$, are stable nodes and the third (x_2, y_2) is a saddle point (see Figure 7). Assume further that the following bifurcation sequence occurs as λ is monotonically increased:

1) For $\lambda < \lambda_1$ the nullclines have a single intersection at (x_3, y_3) which is a stable node and the unique attractor.

2) At $\lambda = \lambda_1$ a saddle-node bifurcation occurs and the (x_1, y_1) node and the (x_2, y_2) saddle point appear. The nullclines are tangent at this complex fixed point.

3) For $\lambda \in (\lambda_1, \lambda_2)$ the three fixed points shown in Figure 7 exist. This is referred to as the trigger regime.
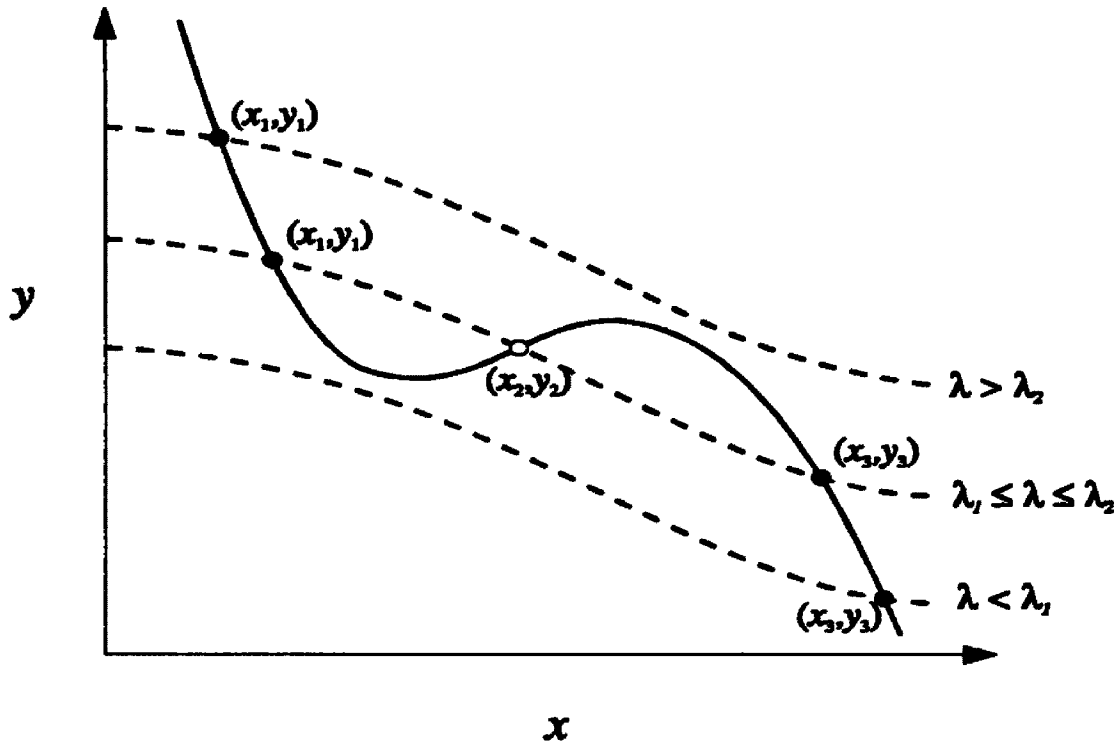
Figure 7. The family of nullclines $f(x,y) = 0$ (solid line) and $g(x,y) = 0$ (broken line). There are three intersections for λ in (λ_1, λ_2). Solid circles correspond to attracting nodes and the open circle to a saddle point.

4) At $\lambda=\lambda_2$ the node (x_1, y_1) and the saddle (x_2, y_2) coalesce in another saddle-node bifurcation, and both disappear. Again the two nullclines are tangent at a complex fixed point.

5) For $\lambda > \lambda_2$ the stable node (x_1, y_1) is a unique attractor.

The analogy in the trigger regime between the dynamic (critical point) structure of

the one and the two-variable systems is apparent. Thus for $\lambda \in (\lambda_1, \lambda_2)$ and with appropri-

ate initial conditions, Equation (9) is expected to have traveling front solutions. This has

been demonstrated numerically in a number of examples [59,22,23,47]. Some analytic

results for similar two variable systems are found in Tyson and Fife [55] and Orteleva

and Ross [42]. Furthermore, since the dynamics of x is fast compared with y ($\epsilon \ll 1$)

and if the spatial distribution of y is close to homogeneous in the part of the front where x

makes the transition from x_1 to x_3, then the direction of front propagation can be changed

by varying λ. For λ close to λ_1 (x_2 close to x_1) the front of x moves in such a way that the

region with x in the basin of attraction of x_3 expands. Alternately, for λ close to λ_2 (x_3

close to x_2) the region with x in the basin of attraction of x_1 expands. The front of x trav-

els in the opposite direction. Finally, because the dynamics of the system depends on λ

in a continuous manner, there is at least one λ, say λ_0 for which the velocity of the travel-

ing front is zero.

The validity of the above analysis was tested by numerical simulation of traveling

fronts in the system of Equation (9) using the x and y parts of Equation (1) for the chemi-

cal dynamics with z replaced by a constant λ. The velocities of traveling fronts initiated

by a (x_3, y_3) pulse were found to be continuously dependent on the assumed value of λ.

However, as illustrated in the one variable system the fronts have zero velocity for a

small range of λ about λ_0 that decreases with the spatial resolution of the calculation.

Furthermore, one can assume some spatial distribution of $\lambda=\lambda(r)$ and demonstrate numerically that the front velocity still approaches zero where $\lambda(r)$ varies about λ_0.

Application To a Three Variable System

Identifying the parameter λ in Equation (9) as the variable z and adding a third differential equation governing z allows the above considerations to be applied to three variables under certain conditions. The space dependent reaction-diffusion system then becomes

$$\frac{\partial x}{\partial t} - D_x \frac{\partial^2 x}{\partial r^2} = \frac{1}{\varepsilon} f(x, y, z)$$

$$\frac{\partial y}{\partial t} - D_y \frac{\partial^2 y}{\partial r^2} = g(x, y, z) \tag{10}$$

$$\frac{\partial z}{\partial t} - D_z \frac{\partial^2 z}{\partial r^2} = h(x, z).$$

This system of partial differential equations is assumed to have the following properties:

1) For $\varepsilon \ll 1$ the x-y subsystem defined by the x and y equations with z as a continuously varying parameter has the bifurcation sequence described above for the two-variable system parameterized by λ. There then will be a trigger regime defined by $z \in (z_1, z_2)$.

2) The values of x and y move rapidly to near one of the stable nodes and closely
follow this node as it moves in response to the slowly varying value of z.

3) The function $h(x,z)$ is such that for large x and small z it is positive and for
small x and large z it is negative. A simple example is $h(x,z)=\alpha x-\beta z$ for ap-
propriate $\alpha, \beta > 0$.

It is easy to find values of α and β such that when the x-y subsystem is near (x_3, y_3), z
increases causing (x_3, y_3) to move toward (x_2, y_2) until these points coalesce and disappear
at $z=z_2$. The system then must move to near (x_1, y_1) where the same values of α and β
cause the evolution of z to change direction and begin to decrease. Eventually z de-
creases to z_2 where the (x_2, y_2) and (x_3, y_3) nodes reappear. As z continues to decrease
(x_2, y_2) and (x_1, y_1) move toward each other until these points coalesce at $z=z_1$, and the sys-
tem must return to near (x_3, y_3). Relaxation oscillations between (x_1,y_1) and (x_3,y_3) occur
in this manner in a spatially homogeneous system if the movement of z takes it below z_1
and above z_2. The homogeneous x-y subsystem is bistable if z remains within (z_1,z_2). By
analogy with the Belousov-Zhabotinsky reaction, states near (x_3,y_3) will be referred to as
excited states while those states near (x_1,y_1) will be called *quiescent*.

If the x-y subsystem is entirely at (x_1,y_1) a local spatial disturbance of it to (x_3,y_3)
while allowing z to remain homogeneous initiates a traveling front in the manner analo-

gous to that described above for one and two variable systems. However, the distribution of z now becomes inhomogeneous in response to changes in the x distribution. The shape and velocity of fronts of x and y are controlled by the distribution of z. In particular, the front of x can change its direction of propagation or stop as a suitable distribution of z develops. This interaction of traveling fronts with an inhomogeneous distribution of z can yield a much richer variety of phenomena than appears in one- and two-variable systems. The reaction-diffusion system now becomes truely dispersive. In order to characterize the effect of this interaction on the form and velocity of traveling fronts in higher dynamical dimensions the following general principle is postulated as a conjecture. It is motivated by and attempts to extend the concepts developed above for one- and two-variable systems where wave fronts are controlled by fixed spatial distributions of some parameter. Similar principles have been used in an implicit form in the analysis of an enzymatic substrate-inhibition system [22,23] and an abstract model of modulated stationary periodic structures [29].

Conjecture

Let z_0 denote the value of z for which the traveling front in the x-y subsystem with z as a fixed parameter has zero velocity. Assume further that (in the x-y subsystem) for $z < z_0$ the front of x moves in one direction as the excited region (close to x_3) expands, and for $z > z_0$ it moves in the opposite direction as the excited region contracts. Let (a,b) be an interval in r on which the distributions of x, y and z are monotonic and $z \in (z_1, z_2)$. If the point $(x,y)_{r=a}$ belongs to the basin of attraction of one node (say (x_3, y_3)) and the point

$(x,y)_{r=b}$ belongs to the basin of attraction of the other node (say (x_1, y_1)) then the form and velocity of the front of x will be determined by one of the following three points:

1) If there exists an interval (a,b) satisfying the conditions above such that the distribution of z is below z_0 on the entire interval, then the distribution of x will evolve to the basin of attraction of (x_3,y_3). When this occurs it will be referred to as an expansion of the excited (close to (x_3, y_3)) region (or contraction of the quiescent region). In this case the "front" of x moves to the right if x is decreasing on (a,b) or to the left if x is increasing on (a,b). See Figure 8.

2) If there exists an interval (a,b) satisfying the conditions above such that the distribution of z is above z_0 on the entire interval, then the distribution of x will evolve to the basin of attraction of (x_1, y_1). When this occurs it will be referred to as contraction of the excited region (or expansion of the quiescent region). The front of x moves to the left if x is decreasing on (a,b) or to the right if x is increasing on (a,b). See Figure 9.

3) If for all intervals (a,b) satisfying the above conditions the distribution of z is equal to z_0 at some point $r_0 \in (a,b)$, then the parts of the distribution of x separated by r_0 will remain in their current basins of attraction. This situation will
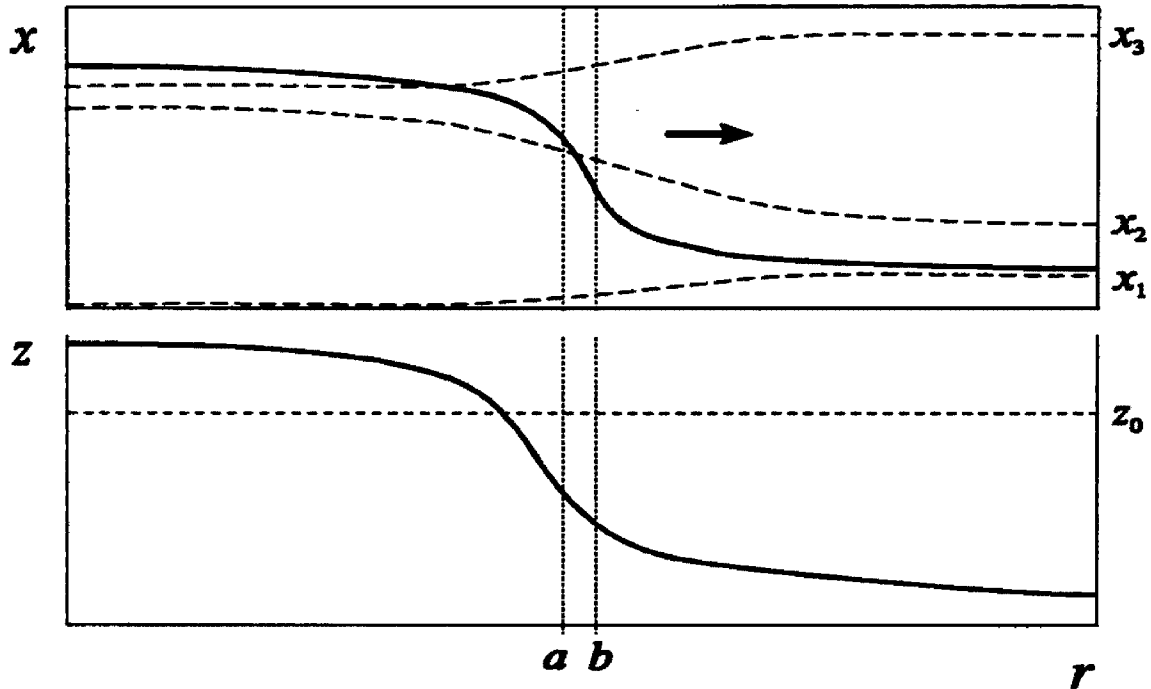
Figure 8. Illustration of the application of case 1 of the Conjecture. The z distribution is completely below z_0 in the region bounded by the interval (a,b). Thus the exicited region expands as the wave propagates to the right.
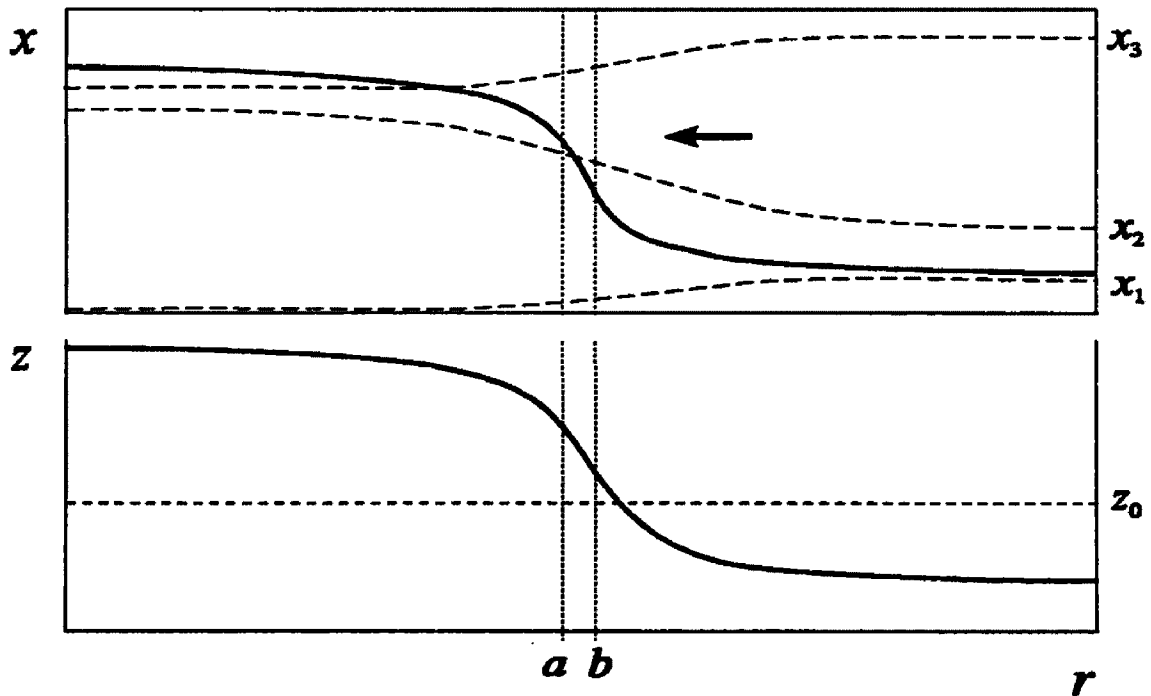
Figure 9. Illustration of the application of case 2 of the Conjecture. The z distribution is completely above z_0 in the region bounded by the interval (a,b). Thus the quiescent region expands as the wave propagates to the left.
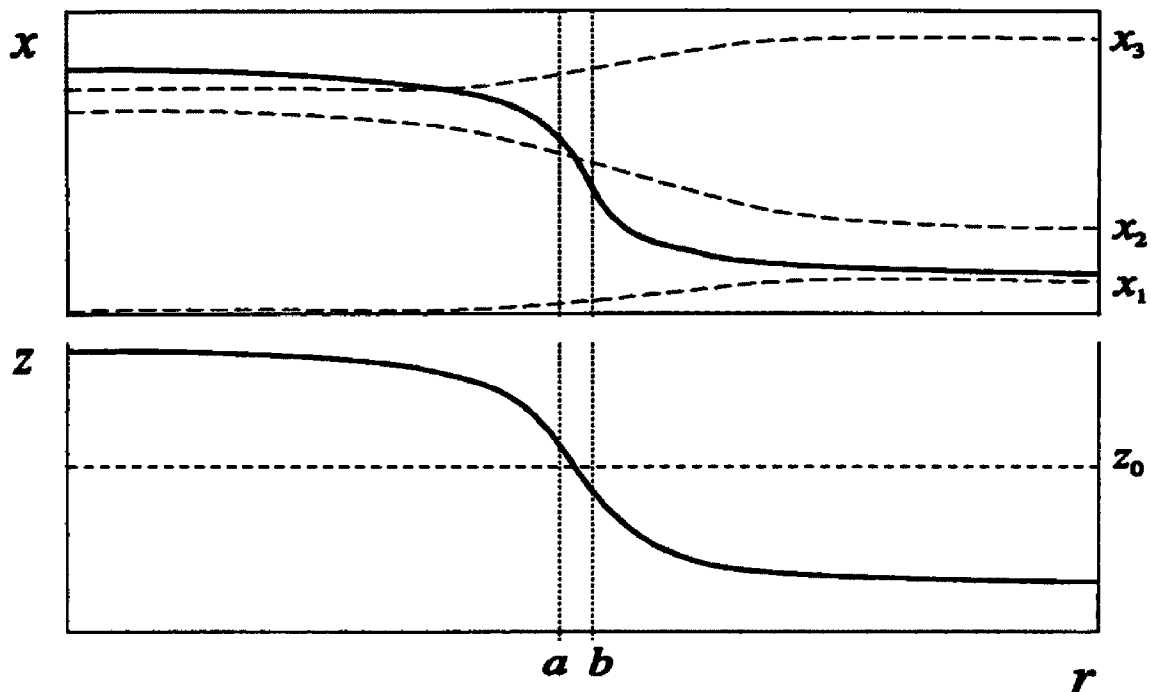
Figure 10. Illustration of the application of case 3 of the Conjecture. All intervals (a,b) will contain the point z_0. The wave in this case is stopped.

be described as the stopping of the front of x. See Figure 10.

In each case the distribution of x will change its shape as it evolves. This conjecture is supported by the numerical results reported above with $\lambda=\lambda(r)$ playing the role of z and by the three-variable calculations reported below. There is some evidence in the three-variable calculations that the conjecture may be exact only if the asymptotic spatial distribution of z about the point where $z=z_0$ is symmetrical. However, the distributions of z in these calculations are sufficiently close to being symmetrical that the conjecture is very nearly quantitatively true.

4. CALCULATIONS - RESULTS OF NUMERICAL SIMULATION

Numerical modeling considerations

The concepts developed above will now be used to describe the evolution of a pattern from a spatially localized disturbance in a numerical simulation of the modified Oregonator model. Substitution of the reaction dynamics for the modified Oregonator, Equation (1), into the general expression for the three variable reaction-diffusion problem, Equation (10), gives the space-dependent model

$$\frac{\partial x}{\partial t} - D_x \frac{\partial^2 x}{\partial r^2} = s\left[y - xy + x\left(1 - \frac{z}{c}\right) - qx^2\right]$$

$$\frac{\partial y}{\partial t} - D_y \frac{\partial^2 y}{\partial r^2} = \frac{1}{s}[-y - xy + fz] \tag{11}$$

$$\frac{\partial z}{\partial t} - D_z \frac{\partial^2 z}{\partial r^2} = w\left[x\left(1 - \frac{z}{c}\right) - z\right].$$

This is a system of three quasilinear partial differential equations in three dynamical variables. Note that the x-y subsystem can be obtained from this model by choosing $w=0$ in the z equation and specifying some initial distribution of z. The diffusion coefficients in Equation (11) are nondimensionalized by the scaling

$$D_i = \frac{\mathrm{D}_i'}{\mathrm{A}\sqrt{k_{M_1} k_{M_3}}}, \text{ for } i = x, y, z.$$

37

Solutions of Equation (11) and its x-y subsystem were approximated using numerical integration by the *method of lines*. In that technique the spatial part of the equations are discretized using second-order central-differencing of the space derivatives on a grid of n equally spaced points. In the case studied here that procedure yielded a system of $3n$ ordinary stiff differential equations whose solutions were approximated by the stiffly stable Gear method [22,25]. Relative local error tolerances for the time integration steps were varied in the range 10^{-5} to 10^{-7} with no detectable change in the solutions. A spatial grid of 250 points was used, and 500 or 1000 points gave essentially the same results. Output consisted of the solution components, time derivatives and error residuals at each space point at equal time increments. The approximate numerical solutions were considered to be asymptotically stationary when the $3n$ time derivatives obtained in the numerical integration procedure were uniformly bounded by some small number (typically 10^{-9}). The appendix describes the software used for these calculations.

The chemical parameter values used in the calculations are shown in Table 1. For these parameters the system is oscillatory with $z_1 = 9.5$, $z_2 = 1174$ and period ≈ 33.5. These chemically reasonable values were chosen so that the homogeneous system was in the oscillatory regime. For this set of parameters Equation (1) satisfies the criteria for application of the above concepts. Because of the time scale separation of the x and z dynam-

Table 1. Model parameters used for simulation of the Modified Oregonator.

$C_{total} = [Ce(III)] + [Ce(IV)]$ (M)	D_x, D_y (cm²/s)	D_z (cm²/s)	f	k_{M5} (s⁻¹)
2.3×10^{-3}	1.0×10^{-5}	3.5×10^{-5}	0.63	0.10
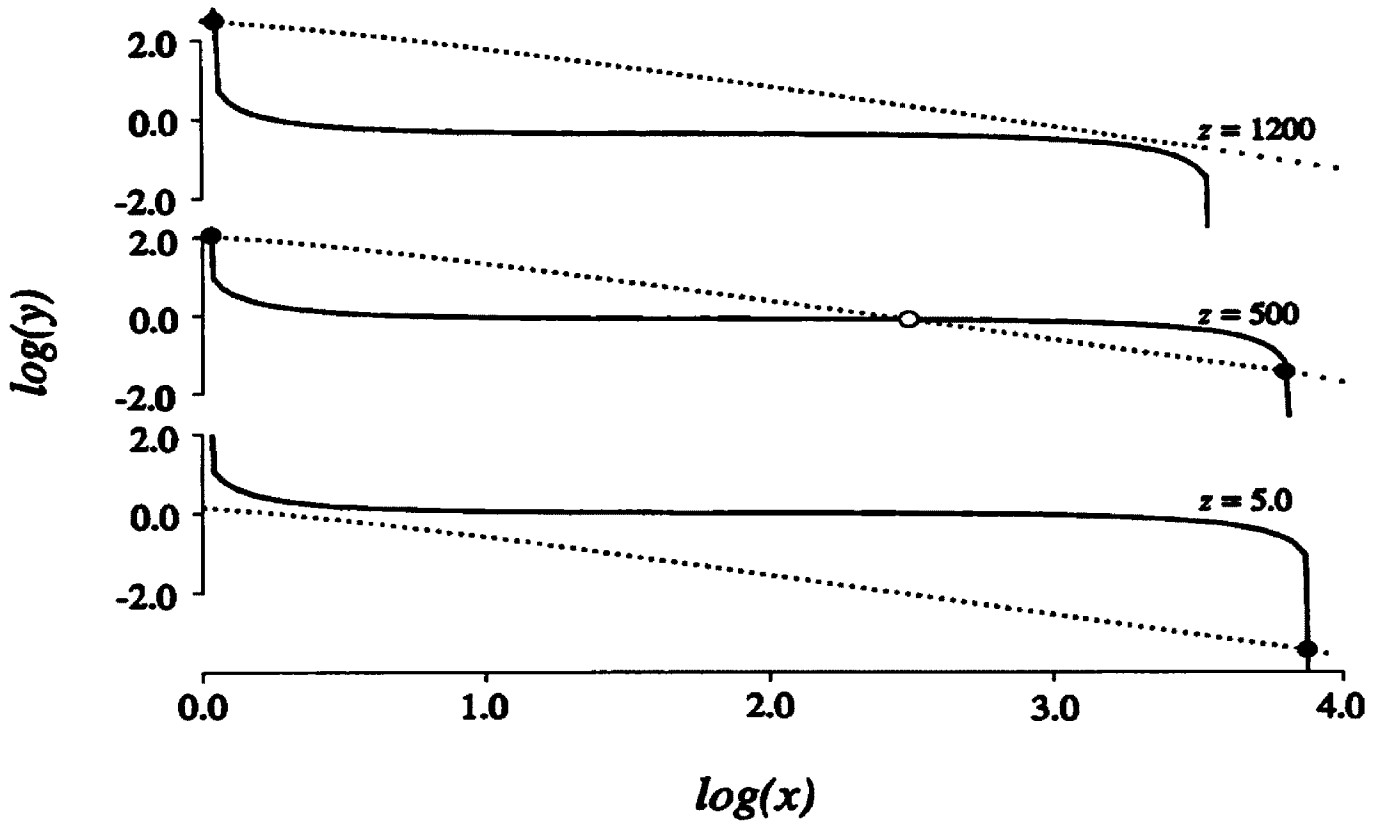
Figure 11. The family of nullclines $f(x,y,z) = 0$ (solid line) and $g(x,y,z) = 0$ (broken line) for the modified Oregonator, Equation (1), with z treated as a slowly varying parameter. There are three intersections and thus a trigger regime for $9.5 < z < 1174$.

ics the z variable may be considered as a slowly varying parameter in the subsystem

consisting of the x and y equations only. The family of x-y nullclines for the subsystem

of the modified Oregonator are shown in Figure 11 for several values of z. The dynam-

ics shown there are qualitatively similar to those of the generalized two-variable system

of Equation (9) (see Figure 7). In particular, the system has unique stable states sur-

rounding an unstable node.

The 2 variable reaction-diffusion subsystem

Before the analysis of the evolution of a pattern can be carried out the quantities z_0 (the value of z which stops the wave in the x-y subsystem), and z_1 and z_2 (the upper and lower boundaries of the trigger regime) must be computed. These three quantities are fixed constants for a particular set of chemical parameters and need only be computed once. The borders for the trigger regime can be determined from the dynamics of the local system by several methods. The path in state space corresponding to the bifurcation sequence described in the two-variable theory above can be traced out using numerical continuation techniques [6]. The points z_1 and z_2 will then show up as saddle-node bifurcations. That method can be checked by algebraically determining the conditions for a polynomial to change its number of roots. This will occur as the system switches from the trigger regime to a single stable node. Finally a reasonable estimate for these quantities can be made by graphical inspection of the nullclines for various values of z. All three methods should be used in each study to ensure the integrity of the values obtained.

The determination of the critical z value for stopping the wave in the subsystem will in general be a more difficult task. The reaction-diffusion equations for the subsystem must be approximately solved for appropriate values of z and the wave velocities measured directly from that solution set. An initial estimate for z_0 can be obtained numerically by simulating a wave in the subsystem while maintaining a linear z distribution. If the initial limits of the linear z distribution bracket z_0 and the stable states for the spatially asymptotic solution are chosen judiciously then the wave will propagate across
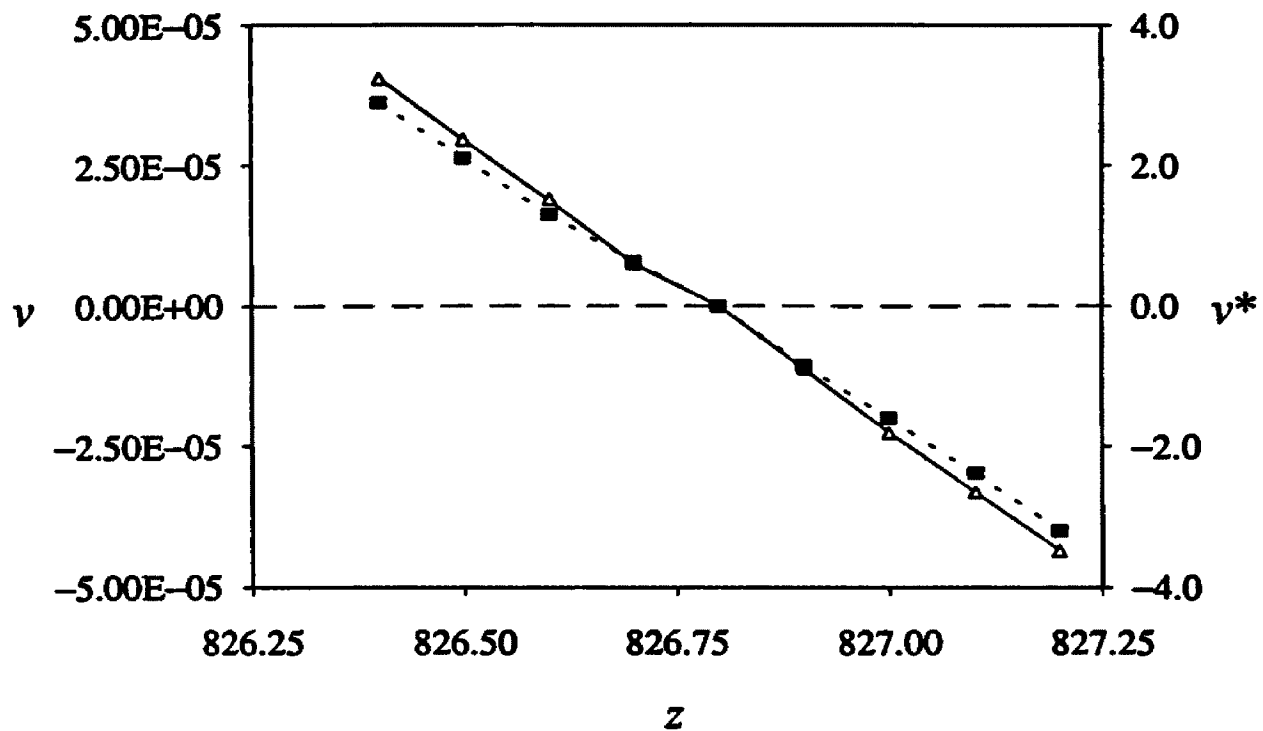
Figure 12. Computation of z_0 for the x-y subsystem with z as a fixed parameter for the modified Oregonator model. The solid line corresponds to v, the wave velocity determined from direct measurement of the solution profiles. The dashed line shows velocity points computed using the maximum temporal derivative obtained in the numerical integration procedure.

the linear z distribution until the front reaches the vicinity in r where the z distribution is close to z_0. Once an initial guess is obtained in this manner the value of z_0 can be refined by bisecting it and measuring the wave velocity directly from the solution data. A good measure of the wave velocity can be obtained from the maximum temporal derivative returned by the integration procedure. Figure 12 shows results for the computation of the z stopping value by both direct measurement of displacement in the solution data set and monitoring of the maximum temporal derivative. Within a constant of proportionality it shows good agreement between the two methods.

The full reaction-diffusion system

The evolution of the homogeneously oscillating three-variable system when it is subjected to a spatially localized perturbation will now be described. That initial disturbance develops into a pulse of excitation. The homogeneous area outside of the pulse is oscillatory, and an additional pulse forms with each oscillatory cycle until a pattern fills the spatial domain. Each new pulse is formed at the interface between the expanding pattern and the oscillatory region. One cycle of this evolution will be described in detail. The evolution to the final pattern occurs by repetition of this cycle until the spatial domain has been filled with a pattern. Calculations were done for the initial-boundary value problem with homogeneous Neumann conditions on the domain [0,L]. The initial conditions were given by the following step functions for x and y with a uniform distribution of z

$$x(r,0) = \begin{cases} x_3, & 0 \le r \le r_0 \\ x_1, & r_0 < r \le L \end{cases},$$

$$y(r,0) = \begin{cases} y_3, & 0 \le r \le r_0 \\ y_1, & r_0 < r \le L \end{cases}, \qquad (12)$$

$$z(r,0) = z_w, \quad r \in [0,L] \ .$$

Here z_w was chosen so as to satisfy the inequality $z_1 < z_w \le z_0 < z_2$ for the x-y subsystem of Equation (1). The stable nodes (x_1, y_1) and (x_3, y_3) for the x-y subsystem were then computed using this z_w. Table (2) shows the geometric constants and numerical values for

these initial conditions.

Table (2). Initial conditions for the integration of Equation (9).

L (mm)	r_0 (mm)	x_1	x_3	y_1	y_3	z_w
5.0	0.08	1.0	5800	180	0.064	600

Thus for $r \in [0,r_0]$ the subsystem is in the basin of attraction of (x_3,y_3) and for $r \in (r_0,L]$ it

is in the basin of attraction of (x_1,y_1). These conditions initiate a traveling front of x mov-

ing to the right since z is below z_0 on some interval (a,b) as defined in case 1 of the Con-

jecture. This is because z increases in the excited region and decreases elsewhere

according to its homogeneous kinetics. At $t = 15$ z exceeds z_2 in the region near $r = 0$,

and the x-y subsystem there begins moving toward the unique attractor (x_1,y_1). As the

distribution of x changes its local curvature (the diffusion term becomes positive) the rate

of fall of x toward (x_1,y_1) is diminished. The narrower the width of the interval where z

exceeds z_2 the larger the diffusion term and the larger this braking effect. As the initially

excited region expands x, and thus z, both slowly decrease in this interval. Figure 13

shows the distributions of x and z at $t=20$. The excited region is expanding to the right

since $z < z_0$ in (a,b).

The distribution of z continues to decrease in the region to the right of the expanding

pulse of x. Figure 14 shows the time evolution of the z distribution as it approaches the

z_1 level at some distance to the right of the expanding front of x. At $t=24$, the distribution

of z falls below z_1 in the region $r>1.5$. A new excited region begins to form there as the
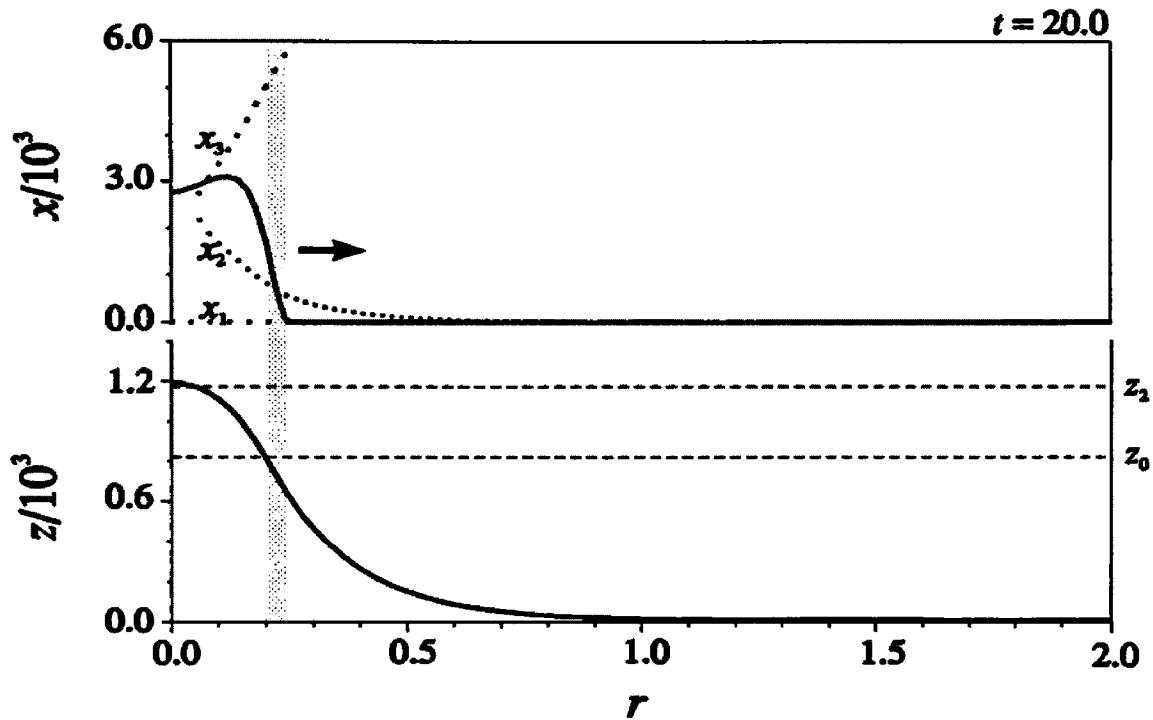
Figure 13. The distributions of x and z (bold lines) at $t = 20$ on the subset [0,2] of the domain [0,5]. The dotted lines denote the values of x_1, x_2 and x_3 for the homogeneous subsystem corresponding to the value of z at that position on r. The dashed lines denote $z_0 = 824$, the value of z that stops the traveling front in the x-y subsystem, and $z_2 = 1174$, the upper border of the trigger regime. The value of $z_1 = 9.5$, the lower border of the trigger regime, is not easily shown on this scale. The arrow indicates the direction of propagation of the x front. The grey area shows the location of an appropriate (a,b) interval for application of the Conjecture. The excited region is expanding to the right since $z < z_0$ in (a,b).

subsystem switches to the (x_3, y_3) basin of attraction. The distributions of x and z at $t=27$

are shown in Figure 15. The distribution of z in the newly excited region is now again

above z_1. A new front[1] appears and moves to the left since $z<z_0$ in (a,b). The front

formed by the initial excitation near $r=0$ still moves to the right as the z distribution is be-

low z_0 in (a,b). As the quiescent region between the two fronts contracts the distribution

---

[1]   A front in this system is rigorously a concentration distribution that covers an infinite domain and monotonically connects (x_1,y_1) with (x_3,y_3). Usually there will be a sharp transition between high and low values of x. However, x is not monotonic in the following, and there are several such jumps of x between x_1 and x_3 in the domain. Each such jump will be referred to as a front.
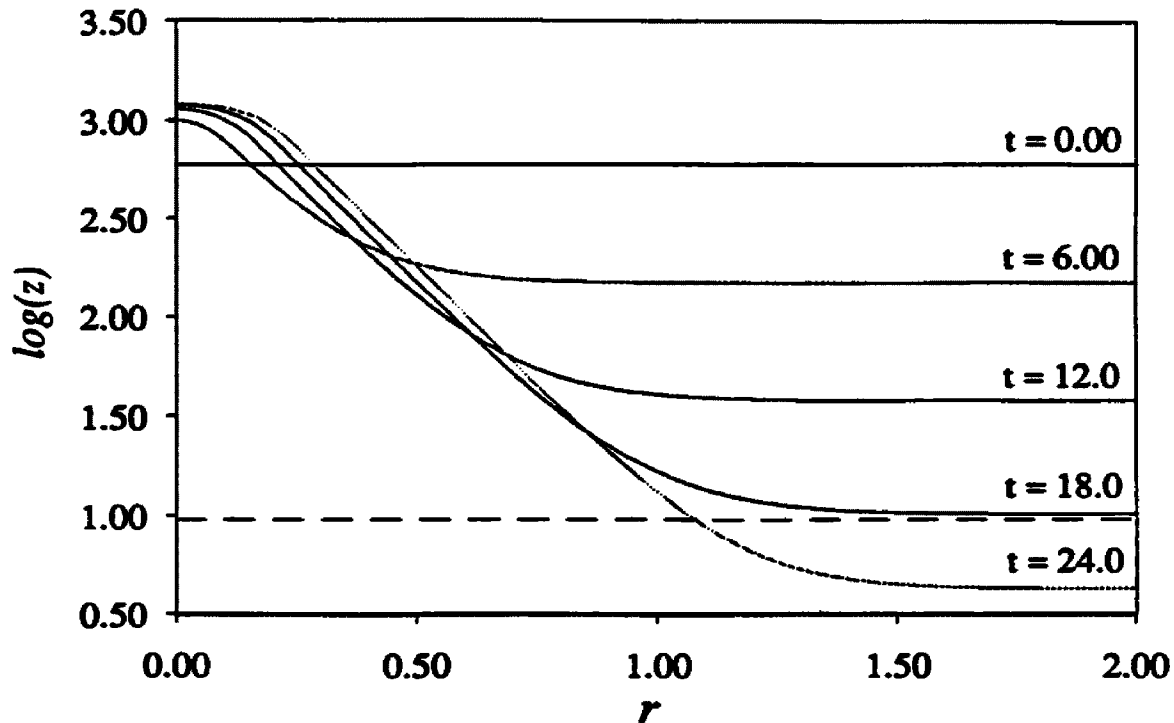
Figure 14. The evolution of the z distribution in the time interval $0 \leq t \leq 24$. In the region close to $r=0$ the z distribution is increasing since the x-y subsystem is close to (x_3,y_3) there. Outside of that region the z distribution is decreasing monotonically in a nearly homogeneous manner because the subsystem is at (x_1,y_1) there. At $t=24$ the subsystem will switch to (x_3,y_3) for $r>1$.

of z increases there. The distribution of z also increases in the region of homogeneous

oscillation as it follows the x motion. The z distribution reaches z_2 at $t=27.6$ for $r > 1.7$,

and the x-y subsystem begins to move almost homogeneously toward (x_1,y_1). The z dis-

tribution then begins to decrease in this region, eventually falling below z_2 at some dis-

tance to the right of the newly formed front. This situation is shown in Figure 16 where

in an interval in which z is above z_2 the distribution of x evolves toward (x_1,y_1). This

leads to a shortening in the interval where z is above z_2 (see Figure 17). The local distri-

bution of x on the right side of this interval is higher than x_2 and is again in the basin of

attraction of (x_3,y_3), so a new front is formed. This front moves to the left since $z > z_0$ in
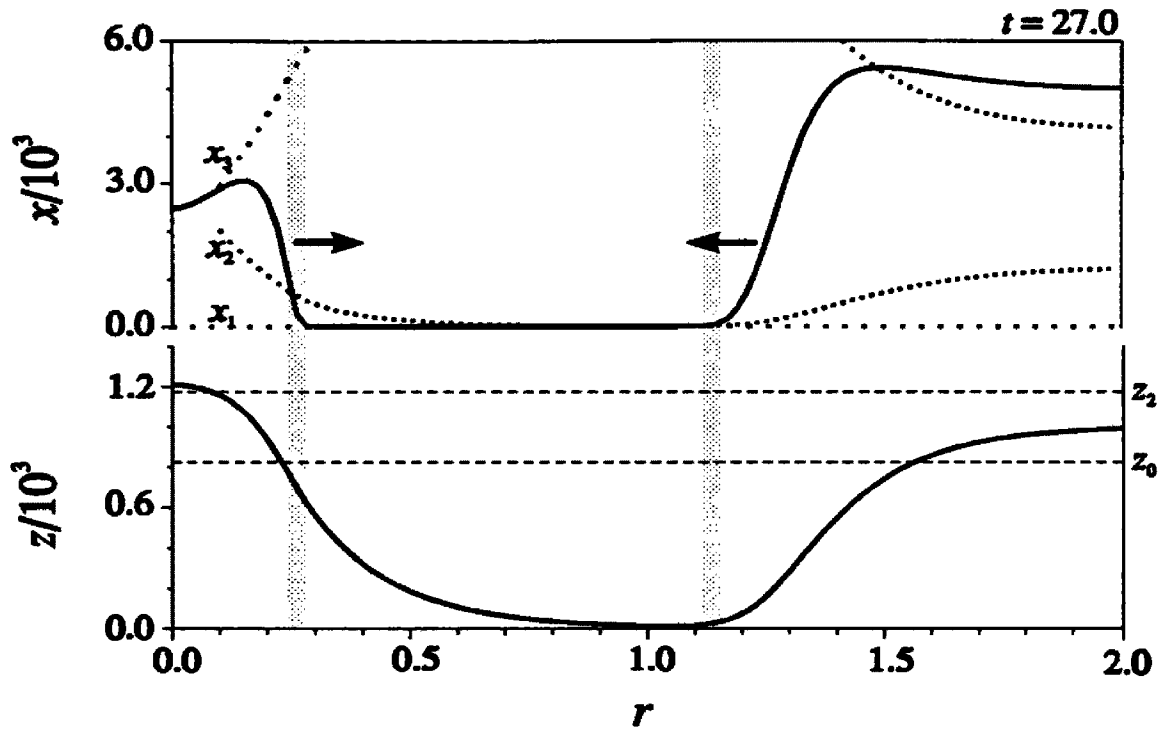
Figure 15. The distributions of x and z at $t = 27.0$. A new front of x moving to the left has been formed as part of the system switches to (x_3, y_3). A quiescent region exists between the two fronts of x. The distribution of z is between z_1 and z_2 except for a small interval near $r = 0$.
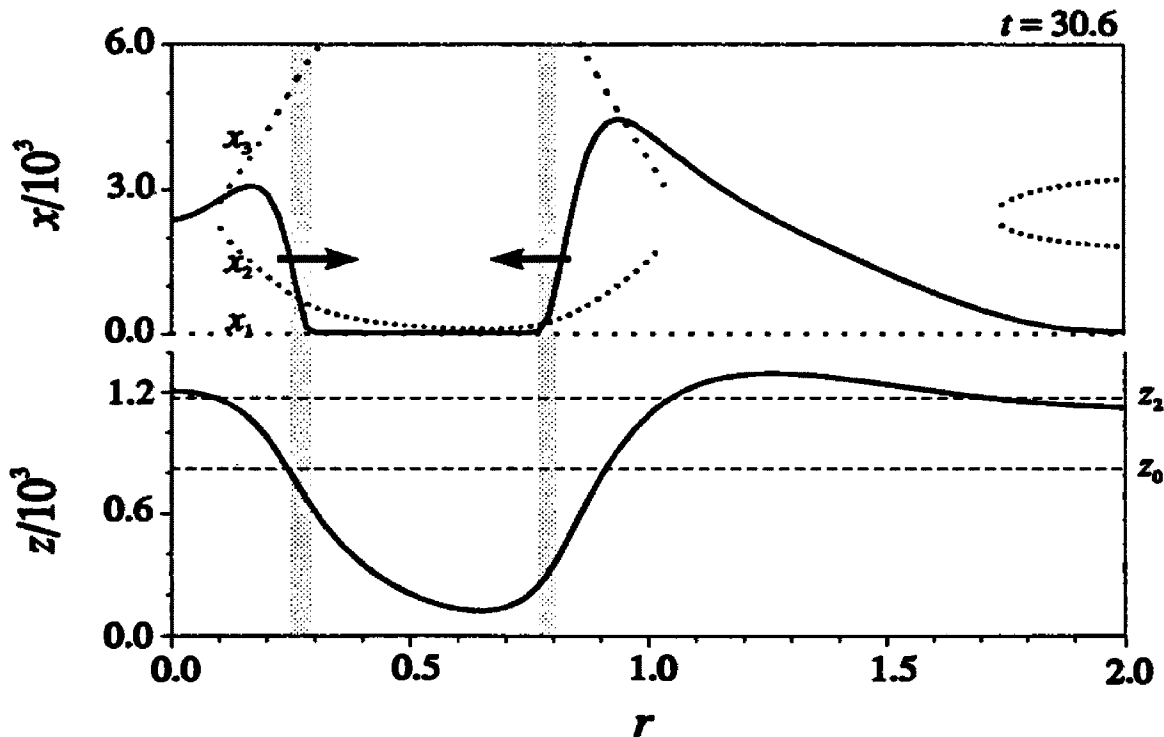
Figure 16. The distributions of x and z at $t = 30.6$. The quiescent region has contracted considerably. The bulk oscillation has switched the distribution of x back to (x_1, y_1). The decaying distribution of x toward (x_1, y_1) is not yet a front as z in most of this region is above z_2.
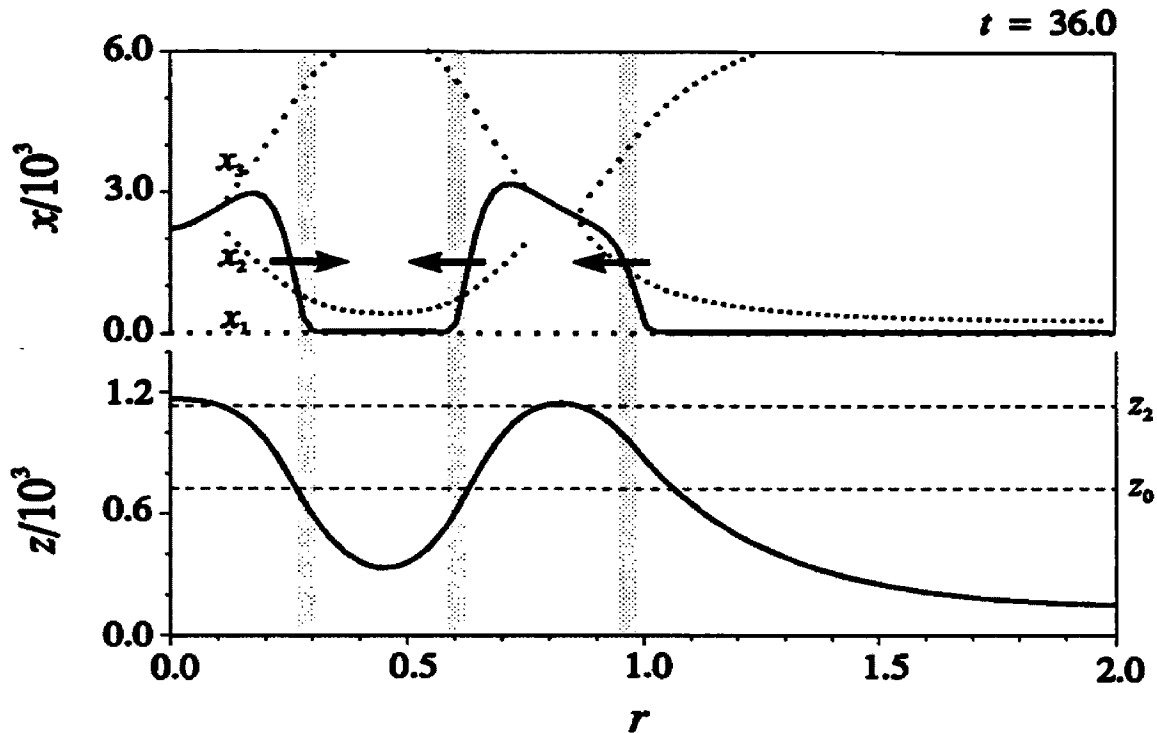
Figure 17. Evolution distribution diagram for $t = 36.0$. The quiescent region is still contracting and the z distribution is increasing there. Another new front of x is formed and moves to the left as z is above z_0 in (a, b). There is still a small region between the two newly formed fronts where $z > z_2$ so that the two fronts have not yet joined to form a pulse.

(a,b). The distribution of z continues to decrease in the region between the two newly formed fronts until it falls below z_2. An excited region in the form of a pulse of high x is now formed, separated from the initial pulse by a quiescent region. Its left front moves to the left as z is still below z_0 in (a,b). However, its right front also moves to the left since $z > z_0$ in its (a,b). The pulse contracts as the velocity of the right front is greater than that of the left front.

The z distribution between the two pulses continues to increase as the quiescent region contracts. The z distribution at $t = 39$ in each of the intervals (a,b) on the fronts that form the boundary of the quiescent region finally exceeds z_0. The contraction of the
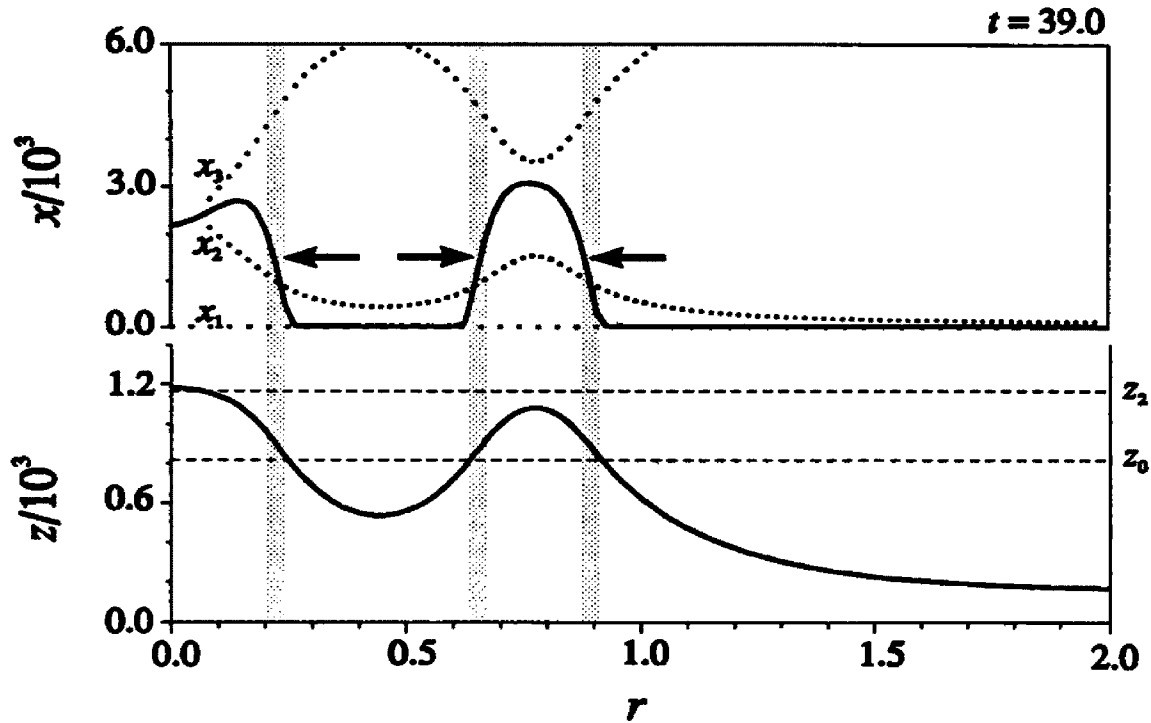
Figure 18. Evolution distribution diagram for $t = 39.0$. The quiescent region is now expanding as z has exceeded z_0 in both (a,b) intervals. The most recently formed front continues to move to the left. A pulse of x now is formed as the distribution of z is below z_2 everywhere between the two newly formed fronts. This excited region contracts.
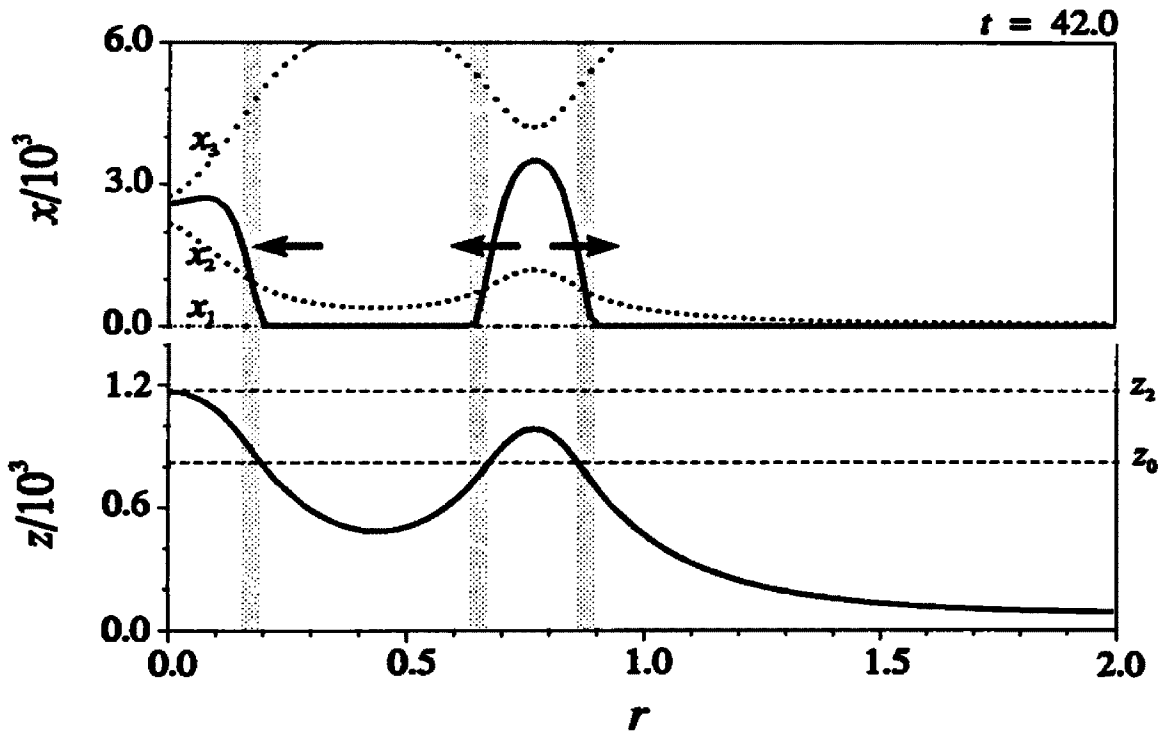
Figure 19. Evolution distribution diagram for $t = 42.0$. The z distribution now is everywhere between z_1 and z_2 and the distribution of x near $r = 0$ is trapped in the basin of attraction of (x_3, y_3). This excited region is still contracting, but will eventually begin to expand. The newly formed excited region expands because z has fallen below z_0 in both (a,b) intervals. Both excited regions eventually stabilize by the mechanism described in the text.

quiescent region is stopped and it begins to expand (Figure 18). As the front in the region of the initial excitation moves to the left, z continues to decrease in the interval near $r = 0$ and at $t = 42$ (Figure 19) finally falls below z_2. At this moment the x distribution in this region is in the reappearing basin of attraction of (x_3, y_3) and thus remains there even as the excited region continues to contract. As a result the z distribution decreases in this region until it falls below z_0 on (a,b) and this excited region expands for a second time. The z distribution in the fronts of the newly formed pulse is now below z_0 in the appropriate (a,b) intervals, causing the pulse to expand.

A mechanism which stabilizes the distributions of x and z in the part of the system to the left of the center of the newly formed pulse is as follows. As the quiescent region contracts the z distribution increases there until it exceeds z_0 in the appropriate (a,b) intervals. At this time the quiescent region begins to expand, thus decreasing the distribution of z there until it again falls below z_0 in the appropriate (a,b) intervals. The quiescent region pulsates with dampening amplitude as it is stabilized. This same self-regulatory mechanism guarantees the stability of the final structure to small perturbations.

The two pulses at (x_3, y_3) are separated by the stabilizing quiescent region. The right front of the newly formed pulse now moves to the right, and the distribution of z decreases ahead of it according to the homogeneous kinetics. At $t = 58.2$ the z distribution again falls below z_1 ahead of this front, and the next homogeneous oscillation is initiated. The process described above for the formation and stabilization of fronts will be repeated
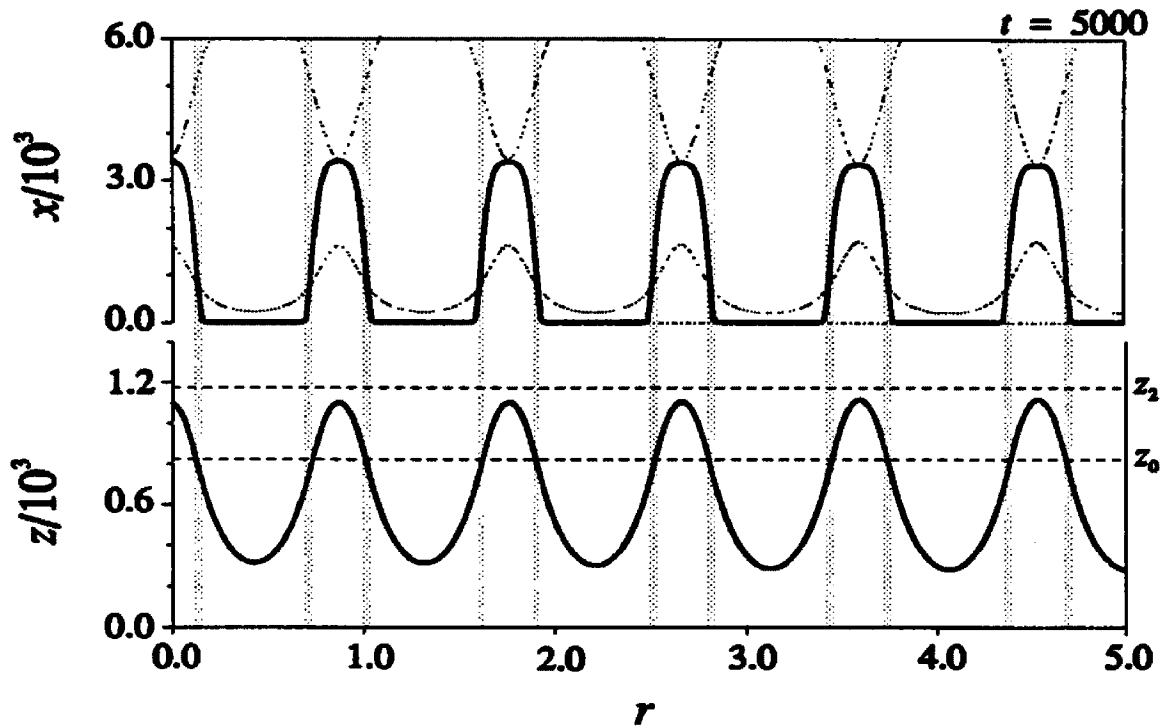
Figure 20. The x and z distributions for the entire domain when the system has reached its asymptotic state at $t = 5000$.

until a spatially periodic distribution of excited pulses separated by quiescent regions

covers the domain at $t \approx 250$. However, the asymptotic pattern which is (arbitrarily) de-

fined as the state when the maximum temporal derivative is bounded by $\varepsilon = 10^{-9}$ is not ap-

proached until $t \approx 5000$. The asymptotic x and z distributions at $t = 5000$ are shown in

Figure 20. The value of z is bounded by z_1 and z_2 (the system is in the trigger regime)

and $z_{min} < z_0 < z_{max}$ as predicted by the qualitative analysis given above.

Figure 21 shows the time-space evolution of the z component of the stationary struc-

ture. The development of spatial periodicity from temporal oscillations is apparent.

Figure 22 shows a cross section of Figure 21 at $r = 5.0$ indicating that z here undergoes

the homogeneous modified Oregonator oscillations (z falls below z_1 and increases above
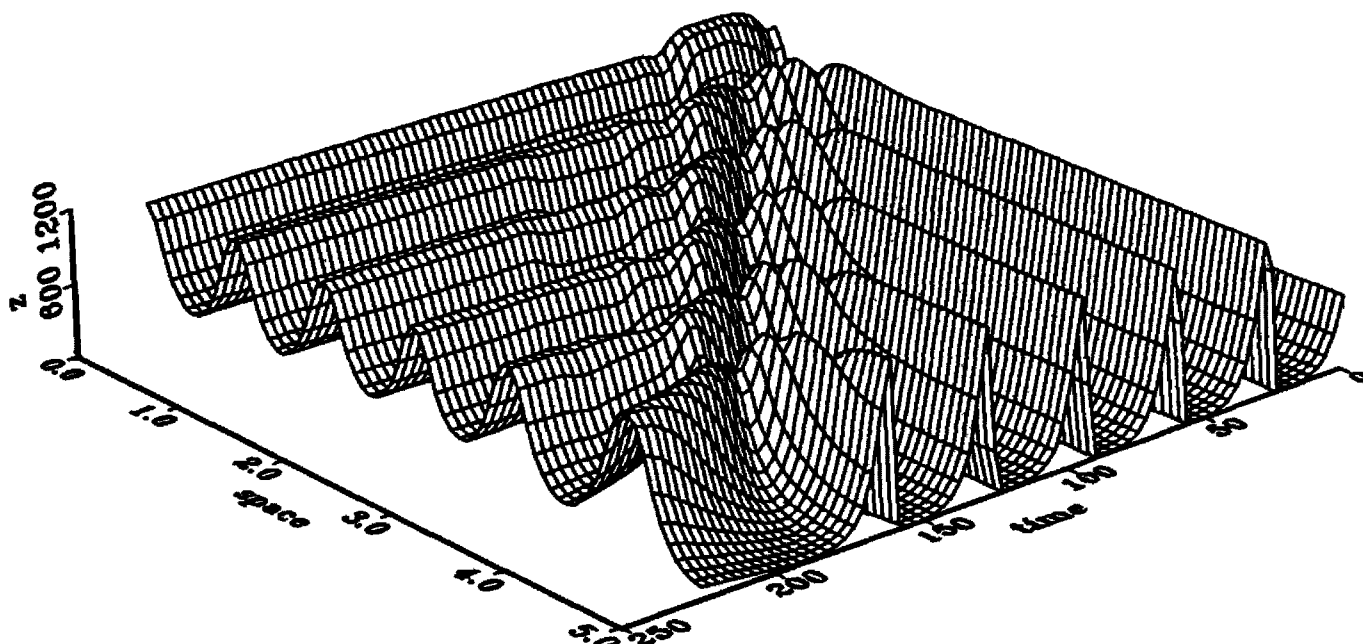
Figure 21. Perspective plot of $z(r,t)$ showing the space-time evolution for a pattern in a homogeneously oscillating medium. Note that the "metawave" nature of the evolution phenomena is evident here as the structure which crosses the plot diagonally across the space-time axes.
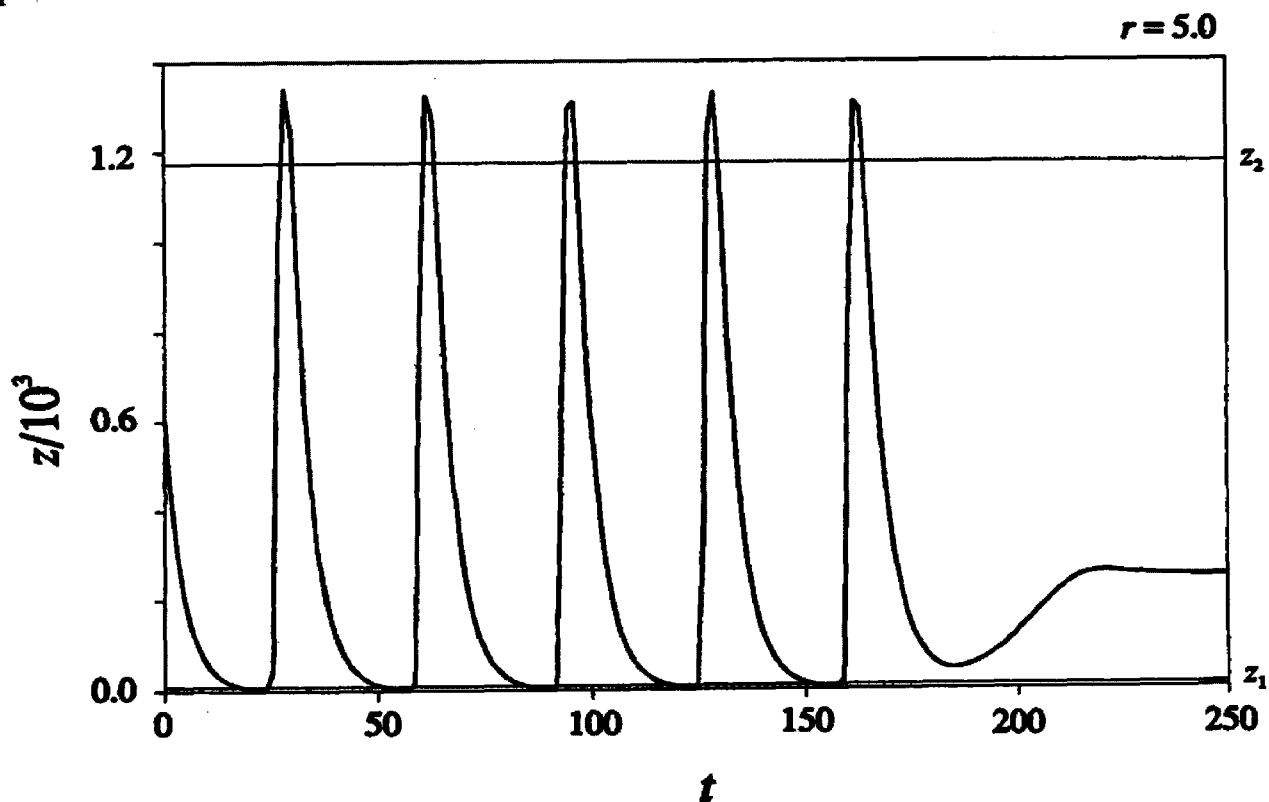
Figure 22. A cross section of Figure 21 at r = 5.0 showing the temporal evolution of z according to the homogeneous oscillation of the modified Oregonator.

z_2) during evolution to the final structure.

The same pattern is approached for a range of initial conditions and does not depend on the width of the initial excitation up to some critical value. However, if the initial pulse is sufficiently broad, then the x distribution near $r = 0$ is trapped in the basin of attraction of (x_1,y_1) rather than that of (x_3,y_3). The resulting pattern is then identical to that in Figure 20 but translated to the right by one-half wavelength. There is also a minimal width below which the initial excitation itself does not survive and system approaches homogeneous oscillation. The pattern obtained does not depend on the values of x and y in the initial excitation provided they are sufficiently close to (x_3,y_3). There is also a range of initial values of z for which the same pattern evolves. The patterns calculated here have an intrinsic length scale that is only slightly affected by boundary effects in a sufficiently large domain. Boundary influences do not have a significant effect on the structure of the patterns obtained here. Their possible effects can be monitored by replicating all results in spatial domains of varying size and spatial grid density. Apart from minor effects on the shape of wave fronts in the regions directly adjacent to the boundaries there was no observed aspect of either evolutionary or asymptotic behavior which showed any strong dependence on the spatial geometry of the systems being studied.

5. DISCUSSION

The evolution observed in the numerical simulations described here are the first example known in which a pattern develops from a local disturbance in a homogeneously oscillating system. These results for this new mechanism of pattern formation overlap two areas of fundamental interest in nonlinear dynamics -- temporal oscillatory phenomena and structures in spatially distributed systems. This phenomena demonstrates a symmetry between patterns in time (oscillations) and oscillations in space (patterns).

A detailed description of the evolution of a pattern in a homogeneously oscillating medium has been given here. The analysis of the system is based on the known principles of wave propagation phenomena in nonlinear reaction-diffusion systems. It was argued that the evolution of these patterns involves traveling fronts joining regions in the basins of attraction of local stationary states (x_1, y_1) and (x_3, y_3). The patterns themselves consist of traveling fronts of x with zero velocity. This evolution to zero velocity is self regulating. It is a result of the general properties of the dynamics of z as given by $h(x,z)$. That is, for x large and z small it is positive (z grows or increases) and for x small and z large $h(x,z)$ is negative (z decreases). Suppose a pulse in the pattern is disturbed in such a way that x is increased in the area of the fronts. This local increase of x will cause z to increase until it eventually exceeds z_0 there. When this happens the fronts will move in a direction opposed to the perturbation. Similarly if a disturbance decreases x in the area of the fronts the dynamics of z will again cause an opposing effect. A disturbance which

53

increases z in the structure will cause a decrease in x. This will cause a decrease in the rate of production of z and thus of z itself. The converse occurs if a disturbance decreases z. Thus the patterns evolved by this mechanism of wave stopping and self-regulation are extremely robust. As a test of their orbital stability the steady state patterns were perturbed by superimposing on them large-amplitude trigonometric and step functions of up to fifty percent of the pattern's maximum amplitude. These large scale disturbances always decayed in a uniform manner back to the steady state pattern. This resilience to external disturbances and extreme robustness of the final structures is a significant aspect of this phenomena.

There are ranges of values of the chemical parameters and diffusion coefficients for which the qualitative features of the evolution to and the form of the pattern are the same as described here. Within these certain ranges the solutions are structurally stable. However, the behavior outside of these ranges is rich and open for exploration. Patterns may evolve in ways other than that discussed here. In some cases multiple oscillations are required to generate each new pulse. In another case a newly formed pulse divides and the secondary pulse bordering the homogeneous region disappears.

Patterns may be found more easily when D_z / D_x is large. No patterns have yet been found in the model described here for $D_z / D_x < 2.5$. This difficulty is not related to a symmetry breaking instability [39] requirement since the initial disturbance breaks the symmetry of the system. It may be related to the *lateral-inhibition* mechanism of pattern formation [8] in which an inhibitor species (Ce(IV) here) must diffuse faster than an acti-

vator species ($HBrO_2$) for a pattern to be stable. However, because of work in another system [61], there is some hope that patterns can be found in model systems for values of $D_z / D_x < 2.5$ and that this may help in determining conditions where they might be found experimentally. Some attempts to mimic the effect of the larger value of D_z by appropriate modification of the chemical dynamics fail because the requirements for front formation are not satisfied.

In general, the diffusion coefficients of small chemical species such as are involved in the BZ reaction are close to 10^{-5} cm^2/s. This may be the reason why reaction-diffusion patterns of the sort described here have not yet been unambiguously observed [42,51] in this system. While it is not possible to accelerate the diffusion rate of chemical species, it is possible to slow this rate in an appropriate medium. Thus Zhabotinsky and Rovinsky [65] have suggested looking for patterns in the BZ reaction in a gel permeation medium where diffusion of the smaller activator species, $HBrO_2$, is slowed relative to that of the larger inhibitor species, Ferroin. Such a slowing of the activator species (I^-) may be responsible [7] for apparent patterns observed [4] in experiments with the chorite-iodide system. The spatial structures seen there show several characteristics of those expected to arise from true Turing-type diffusive instabilities.

After having expounded an extremely detailed description and analysis of this pattern formation phenomena in terms of interactions of multiple wavefronts in a dispersive medium it may be worthwhile to look at it from a larger, more abstract and general perspective. One approach to this may be to consider the bulk medium in terms of the existence

of three distinct states or phases segragated in space but interacting in time. These phases might be classified in the following manner: one which is spatially uniform but temporally active (the oscillatory region), another which is in a stationary steady state but nonuniformly distributed in space (the region where the pattern has formed) and finally the interface between these two regions. This interface region is the active area where the transformation from an oscillatory to a stationary nonuniform state is carried out. This active, interfacial region propagates through the medium with a velocity that depends on the dynamics of the mixture in a complicated way. The propagation of this active region across the domain is very apparent when the simulation data is viewed in a time animation sequence or from a surface perspective graph such as that in Figure 21. In the data set described in this report this *metawave* travels through the domain at an approximate rate of 5 space units per 250 time units. This velocity is orders of magnitude greater than the front velocities in the detailed evolutionary process described above. It's possible that this disturbance or active region propagates as a kinematic wave. What factors in the dynamics of this system might control its rate? In the simple evolution described here (a single oscillation yields a single pulse) the temporal oscillatory period is a large factor, but it was mentioned above that pattern formation mechanisms of considerably more complexity have been observed numerically in this system. These mechanisms range from multiple oscillations per pulse to the formation of multiple pulses per oscillation. Thus other important factors must be at work here. They would probably include the transport coefficients and the multiple time scale separation constants. In particular the

role of the catalyst or inhibitor species could be important here. It should be noted that though it plays a fundamental role as a switch for oscillations and velocity control for wave motion the catalyst species does not itself propagate as a dynamical wave. Its motion might be more acurrately characterized as shadowing the wave motion of the activator species. In this respect its motion may be closer to that of a kinematic or phase wave. The important part that inhibitor and catalyst type species play in these dynamic phenomena could result from some intimate connection with the large scale kinematic behavior of the abstract transport process in the three-phase system. An understanding of the catalyst's role there could possibly clarify the various types of evolution observed in the system studied here as well as shed some light on the problem of diffusion coefficient magnitudes.

6. SUGGESTIONS FOR FURTHER RESEARCH

Future research efforts in this subject should concentrate on the following areas. They fall into two main categories: correcting deficiencies in this work and extending this work in several new directions.

A better scaling scheme for the modified Oregonator should be developed. The scaling used here and in previous work on the space dependent Oregonator leaves the space term in dimensioned form. This is contrary to the accepted practices of analysis of differential equations and probably does not give the analytically simplest mathematical form to the model. An improved scaling for the system should show the time scale separation which clearly exists in this model more explicitly and possibly eliminate an additional parameter.

There is very little fundamental analytical rationale to justify the extension of the one variable theory of reacting and diffusing systems to two dynamical variables. The approach used here to justify such an extension is primarily to make the two variable system as "one-dimensional" looking as possible by making assumptions about its dynamics. This is similar to the approach used by Fife [17] who analysed stationary structures in an abstract activator-inhibitor system and Tyson and Fife [56] in their work on wave phenomena in a two variable model of the BZ. That work used asymptotic methods and singular perturbation techniques to rationalize their assumptions. Though much numerical

58

analytical evidence exists to support this theory, better rigorous analysis of wave phenomena in two variable reaction-diffusion systems should be carried out.

Further analysis of The Conjecture is needed. Numerical evidence and qualitative analyses presented here and elsewhere have given support to the validity of The Conjecture. But to put the theory on firm ground an analytical proof of it should be given. This is a nontrivial task, however, to analyse nonlinear reaction-diffusion type systems in more than one-dynamical dimension. The numerical evidence presented here supports the validity of the Conjecture for the particular model system used in this study. Further experimental support for it would come from the demonstration of its validity in other kinetic models for wave phenomena.

This mechanism of pattern formation should be investigated in the context of other models of the BZ. Such studies would reinforce the idea that the types of phenomena described here are associated with the BZ reaction rather than mere artifacts of the modified Oregonator model. In particular, the Tyson-Fife two-variable Fe catalyzed model may be better suited for mathematical analysis because of its simpler form. That model has been used successfully for the analysis of scroll waves, spiral waves and target patterns in the BZ. Thus there may be reason to believe that it could also exhibit the types of behavior reported here.

REFERENCES

Appendices

A. Software for analysis of reaction-diffusion systems

A necessary part of a research project of this nature is the design and implementation of software tools for the efficient and accurate computation of the quantities of interest to the study. Processing and analyzing the resulting data require programs that maintain the integrity of the data and optimize the extraction of useful information from the data. Brief descriptions of some of the important software developed for this project will be given in this appendix. Appendix B describes in detail a FORTRAN callable graphics library designed to allow the user the capability to integrate data plots directly into their existing computational software.

All of the software described in these appendices was written by the author of this report and is available through Dr. Richard J. Field at the Dept. of Chemistry, University of Montana.

RDSOLVE

This is a front end for the LSODE ordinary differential equation integration engine. It is used when systems are derived by discretization of partial differential equations. The user must supply a subroutine specifying the problem dynamics at link time. Model and control parameters can be input either interactively or read in from a file. The study of the temporal development of spatially distributed systems puts a heavy load on disk

60

I/O and storage capabilities. Much time can be dedicated to moving data around on the relatively slow magnetic-mechanical devices. This program tries to minimize that overhead by using block buffered disk I/O and processing and storing all output data in binary format. This has the additional advantage that critical data can only be accessed in a programmatic manner which helps to ensure a high degree of data integrity. Binary output data can be processed using the program RDVIEW which is described below. During computational runs the status of the calculation can be monitored either graphically or in character mode. Status information can be updated at user defined intervals and includes graphical solution profiles, progress indicators and integration control status (including integration stepsizes, orders, number of function evaluations, etc). The researcher may choose to have output consisting of an integration status log for the entire run, solution components for all variables, time derivatives of any order up to the order of the last integration step and error residuals. The program is available in portable FORTRAN 77 source code. Runtime graphics display capability is only supported under Micrsoft FORTRAN 4.0 or above and requires the AG2TEKPC graphics library.

STIFFODE

This is a front end for LSODE stiff integration engine. It is similar to RDSOLVE but for systems of stiff ordinary differential equations without a band structured Jacobian. It is available in FORTRAN 77 source code with graphics modules for Microsoft FORTRAN 4.0 and above. It requires the AG2TEKPC scientific graphics library described below.

RDVIEW

This program allows viewing and processing of binary output data from RDSOLVE. It is available in executable form or Microsoft FORTRAN 4.0 or above source code form. It requires the AG2TEKPC scientific graphics library described below.

AG2TEKPC

This is a FORTRAN callable library of hardware specific assembly language graphics functions for PCs which is optimized for use on mathematical and scientific problems. It is available as a library of object modules for linking with user created FORTRAN programs. A detailed description of this library is given in Appendix B.

Miscellaneous programs

XZ-DISTR	Displays the spatial distribution of two solution components simultaneously and computes and shows the nodes at each spatial grid point using the value of z at that point.
NULLS	Computes nullclines for the x-y subsystem
ZRANGE	Computes z_1 and z_2
CONCSURF	Draws surface perspective plots from RDSOLVE data
RDTO3D	Convert RDSOLVE output data to ASCII format for 3D plotting
XYVIEW	ASCII data file graphical viewing facility

B. AG2TEKPC - Scientific graphing package for PC's

The following is a description of the AG2TEKPC library of scientific graphics routines which was designed and implemented by the author of this report.

AG2TEKPC: Microsoft FORTRAN callable graphics library
Revision level: Version 1.1 June 1990
Author: William S. Comstock, Jr.

The AG2TEKPC library is a collection of Microsoft FORTRAN 4.0 callable graphics routines optimized for scientific applications. It emulates the many of the functions provided by the Tektronix AG2TEK PLOT 10 graphing package. Programs calling the routines run on IBM PC/AT and compatible computers with EGA or Hercules (HGC) graphics displays. The package was originally developed as a tool for porting graphics applications for study of reaction-diffusion systems from mainframes running Tektronics PLOT 10 but finds more use now as a general purpose FORTRAN callable graphics library for the PC. The library consists of two groups of subroutines: TCS and PLOTA. The collection of Terminal Control Routines (TCS) is a subset of those provided by PLOT 10. These routines also include a set of display specific routines for manipulating images in the PC graphics environment in a way which is not possible on the 4010 type terminals. This package also provides a set of high level data graphing functions analogous to those contained in the PLOT 10 Advanced Graphing II package. Each of these sets of routines are described below.

Contents of the distribution disk:

AG2DEMO.FOR	Example program using AG2TEKPC graphics
AG2PLOTA.INC	Include file for high-level graphics routines
AG2TCS.INC	Include file for TCS routines
AG2TEKPC.LIB	Library of graphics subroutines
AG2TEKPC.MAN	Documentation for the library
FORUTIL.LIB	Library of miscellaneous FORTRAN utilities
GRAPHEGA.LIB	Library of device specific routines for the EGA display adapter
GRAPHHGC.LIB	Library of device specific routines for the HGC display adapter

System requirements

To use the library your computer must be an IBM compatible operating under MS/PC-DOS 2.0 or higher with an EGA or Hercules display adapter. The subroutines are designed to be called only from Microsoft FORTRAN version 4.0 or above.

Note on use of the library

Application programs calling these procedures must be linked with the AG2TEKPC library as well as the device specific library GRAPHxxx where xxx is EGA or HGC (Hercules) depending on the graphics hardware environment. The libraries AG2TEKPC and GRAPHxxx may be combined using the Microsoft Library utility. The command syntax for this operation is:

        lib AG2TEKPC+GRAPHxxx.lib;

This will append the device specific functions to the AG2TEKPC library. See the file AG2DEMO.FOR for an example of the link operation syntax.

Notes on Tektronics PLOT 10 compatibility

- Device (virtual) coordinates are defined in the range $0 \le x \le 639$ and $0 \le y \le 349$ (EGA) or $0 \le x \le 719$ and $0 \le y \le 347$ (HGC).

- Graphics mode text I/O. A subset of the PLOT 10 alphanumeric functions are implemented here. Their arguments are passed as character types as opposed to the integer types used in PLOT 10. These routines are intended to provide support for tasks such as labeling graphic data and prompting for and accepting user input. The library is not designed for tasks involving massive text processing such as writing text editors, word processors, etc. Therefore control over text margins, tabs, etc. is not provided.

- It's not clear to the Author that the concept of output buffering is useful in the PC graphics environment. Therefore the following TCS functions which control terminal output buffering are not supported in this implementation: ANMODE, LEFTIO, RECOVR, SEEBUF, SETBUF and TSEND.

- The package does not include routines for scaling or rotations of virtual vectors, segmented or incremental plotting modes, display units conversion or monitoring and control of Terminal Status variables.

- The following routines are implemented only as stubs and may be called from the library with no effect: ANMODE, PLON, PLOFF, WAIT62.

Notes on programming

- Application programs calling the AG2TEKPC routines must be compiled as Microsoft "large" memory models. This is the default memory model for Microsoft FORTRAN.

- For programs which must run on both mainframes using PLOT 10 and PC's maximum portability is obtained when all graphics output is done in the user's virtual data space (the space of real coordinates representing the problem).

- The use of FORTRAN I/O statements (READ, WRITE) should be avoided in graphics modes. Their use may result in unpredictable display behavior. Optimal display speed and control is obtained when using the TCS routines TINSTR, ANCHO, ANSTR and FWRITE for terminal I/O.

- All integer arguments to TCS function are declared as two byte integers (integer*2). Use of the /4I2 compiler switch will guarantee that all integer constants and variables declared with the integer type use two bytes of storage.

- The files AG2TCS.INC and PLOTA.INC contain interface statements for all of the routines in the AG2TEKPC library. Including these files at the beginning of each source code file containing calls to the library will guarantee that the argument types match those of the subroutines. The Microsoft FORTRAN compiler will generate warning messages for any data type mismatches between subroutine dummy arguments and actual calling parameters. Good programming practice suggests that all variables be explicitly declared. The /4Yd compiler switch will force type checking by giving warning messages for any undeclared variables in the source module. Note that the /4Yd switch will not provide checking of subroutine dummy arguments. These must be carefully checked manually.

New features in version 1.1

- Support for Microsoft compatible mouse.

- Vertical text output.

- Full bit block operations.

- Graphics mode video paging control (EGA only).

- Video read capability.

TCS functions

The following routines provide a reasonable emulation of the Tektronix 4010A01
PLOT 10 Terminal Control System (TCS) in the IBM PC graphics environment:

ANCHO	DSHREL	MOVEA	SEEDW
ANSTR	DWINDO	MOVER	SEELOC
CSIZE	ERASE	MOVREL	SEETW
DASHA	FINITT	NEWPAG	SVSTAT
DASHABS	HDCOPY	PNTABS	SWINDO
DASHR	HOME	PNTREL	TINPUT
DRAWA	INITT	POINTA	TINSTR
DRAWR	LINHGT	POINTR	TWINDO
DRWABS	LINWDT	RESTAT	VCURSR
DRWREL	MOVABS	SCURSR	VWINDO

Extensions to the TCS functions

The library includes extensions to the TCS functions. Those procedures utilize hardware
specific features of the EGA and HGC adapters and are not compatible with the
Tektronics PLOT 10 library or the Tektronics graphics terminals. A detailed listing of
the available subroutines and functions is given below.

PLOTA - Graphics Applications Functions

The PLOTA routines are high level functions for displaying data graphically. They set
up scaled display windows with labeled axes and tic-marks and allow the caller to plot
individual points or sequences of points in the defined display area. They may be used
alone or in conjunction with the lower level TCS routines. These routines are analogous
to those in the PLOT 10 Advanced Graphing II package. A detailed listing of the
available subroutines and functions is given below.

Extensions to the TCS Functions

The following list shows the extensions to the TCS functions. For each procedure the declaration and a brief description of its function and definitions of the parameters is given.

SETCLR

```
subroutine setclr(ivalue)
integer*2 ivalue
```

Set the drawing color to *ivalue*. Allowable color values are in the range 0 to 15 (default EGA palette). On the HGC 0 is pixel off and 1 through 15 are pixel on.

PNTVAL

```
integer*2 function pntval(ix, iy)
integer*2 ix, iy
```

This routine returns the value of the pixel located at virtual screen coordinates *ix*, *iy*. Values returned are palette numbers 0 through 15 for EGA and 0 (pixel off) or 1 (pixel on) for the HGC adapter. Does not update the graphics beam position.

TEXDIR

```
subroutine texdir(path)
integer*2 path
```

Set graphics text output for horizontal (0) or vertical (1) path. Default is horizontal.

FWRITE

```
subroutine fwrite(ix, iy, x, fmt)
character fmt(1)
integer*2 ix, iy
real*4 x
```

This function provides FORTRAN-like formatted output of numeric data in graphics mode. The numeric input data (*x*) is displayed right justified and padded with leading spaces at beam position *ix,iy* (virtual device coordinates) as specified in the format string (*fmt*). The acceptable format specifications are a subset of the FORTRAN formats: Iw, Fw.d & Ew.d where w is total field width, d is number of decimal digits following the decimal point and I, F, and E call for integer, fixed point and floating point formats. Input number must be real*4 - an integer value may be output by passing float(i) with an I format specifier. Maximum field width is 20. Does not update the graphics beam position.

Notes on use of subroutine fwrite:

1. Minimal checking of input argument validity is performed. Make sure that x is a valid real*4 number, the format string is properly specified and that the field width does not exceed 20.

2. Optimal output efficiency is obtained when the screen position is "byte aligned". That is when the screen horizontal coordinate is a multiple of eight.

SETAPG

```
subroutine setapg(ipage)
integer*2 ipage
```

Set Active Page. The EGA video buffer is large enough to hold two full screens of graphics data. These two regions of video memory are referred to as "video pages" and are numbered 0 and 1. This routine selects the page (active page) to which graphics output is written. The active page need not be the currently displayed page (visual page). The default active page is page 0. This routine will have no affect on the HGC.

SETVPG

```
subroutine setvpg(ipage)
integer*2 ipage
```

Set Visual Page. This routine selects the region of EGA video memory which is currently displayed (the visual or display page). The default visual page is page 0. This routine will have no affect on the HGC.

SAVBLK

```
subroutine savblk(minx, maxx, miny, maxy, buffer)
character buffer(1)
integer*2 minx, maxx, miny, maxy
```

Save the rectangular block of pixels to the character array buffer.

Notes on bit block operations:

1. The rectangular block is defined by its lower left (*minx*, *miny*) and upper right (*maxx*, *maxy*) corners (screen coordinates).

2. The buffer size must be at least $N*(DY+1)*((DX/8)+1) + 5$ bytes where N is 4 for EGA and 1 for HGC and DX, DY are the number of horizontal and vertical pixels in the block.

3. It is the caller's responsibility to allocate sufficient space in the buffer to hold the block. Failure to do so may produce unpredictable results.

4. Block operations cannot be performed on blocks which re quire buffers larger than 64K. To operate on larger blocks use 2 consecutive bit block operations. There is minimal overhead for 2 operations.

5. Bit block operations do not change the terminal status.

```
subroutine resblk(buffer, ix, iy)
character buffer(1)
integer*2 ix, iy
```

Restore the rectangular bit block previously saved with SAVBLK to the screen. The block is positioned with upper-left corner at screen coordinates ix, iy. See notes under SAVBLK for definitions of other arguments and notes on use of bit block operations with AG2TEKPC.

```
subroutine copblk(minx, maxx, miny, maxy, ix, iy, buffer)
character buffer(1)
integer*2 minx, maxx, miny, maxy
integer*2 ix, iy
```

Copy the defined block to the position with upper-left corner at screen coordinates ix, iy. See notes under SAVBLK for definitions of other arguments and notes on use of bit block operations with AG2TEKPC.

```
subroutine movblk(minx, maxx, miny, maxy, ix, iy, buffer)
character buffer(1)
integer*2 minx, maxx, miny, maxy
integer*2 ix, iy
```

Move defined block to position with upper-left corner at screen coordinates ix, iy. See notes under SAVBLK for definitions of other arguments and notes on use of bit block operations with AG2TEKPC.

```
subroutine filblk(minx, maxx, miny, maxy, value)
integer*2 minx, maxx, miny, maxy
integer*2 value
```

Fill the defined block with color.

```
subroutine scrsiz(nxpix, nypix)
integer*2 nxpix, nypix
```

Returns the number of screen pixels in the horizontal (*nxpix*) and vertical (*nypix*) directions.

PLOTA - Graphics Applications Functions

The PLOTA routines are high level functions for displaying data graphically. They set up scaled display windows with labeled axes and tic-marks and allow the caller to plot individual points or sequences of points in the defined display area. They may be used alone or in conjunction with the low level TCS routines. Procedures are also available for user customization of the displayed graphs. These routines are analogous to those in the PLOT 10 Advanced Graphing II package and are extensions of the routines in the SIMDRW package developed by Richard J. Hayden at the University of Montana Department of Physics.

WINDOW

```
subroutine window(nx, ny, xmin, xmax, ymin, ymax, k)
integer*2 nx, ny, k
real*4 xwmax, xwmin, ywmax, ywmin
```

Initialization procedure sets up plotting area and draws graph frame with labeled tic marks and axes. This routine should be called before the actual data plotting routines.

Input parameters:

nx,ny	Number of tic marks along the coordinate axes.
xmin,xmax	Minimum, maximum data values along the x-axis.
ymin,ymax	Minimum, maximum data values along the y-axis.
k	Not used at this time.

Note that the default plot options may be changed by the user through calls to the *setxxx* procedures described below.

```
subroutine genplt(x, y, nstrt, nstop, k, mode)
integer*2 k, mode
integer*4 nstrt, nstop
real*4 x(1), y(1)
```

Plots a series of data points using various symbols or line types.

Input parameters:

x,y   arrays of coordinates of the points to be plotted.

nstrt   array index of the first point to be plotted in *x*, *y* arrays.

nstop   array index of the last point to be plotted in *x*, *y* arrays.

k   Not used.

mode   Specifies type of plot:

   1 - line plot (solid)

   2 - line plot (long dashes)

   3 - line plot (short dashes)

   4 - line plot (dotted)

   5 - point plot (dots)

   6 - point plot (squares)

   7 - point plot (diamonds)

   8 - point plot (plus signs)

   9 - point plot (x's)

   32 < *mode* < 128 - point plot (*mode* is ASCII character code)

```
subroutine symbol(x, y, k)
integer*2 k
real*4 x, y
```

Draws a symbol at the point (x,y).

Input parameters:

x,y   Coordinates of the point at which symbol is drawn.

k   Symbol type code as follows:

  1 - square

  2 - diamond

  3 - plus sign

  4 - cross (x)

  $32 < k < 128$ - ASCII character *k*

PAUSE

```
subroutine pause
```

Beeps the system speaker and pauses execution of the calling program pending keyboard input. Alt-P dumps the graphics screen to an Epson compatible graphics printer, any other key resumes processing, erases the screen and switches to alphanumeric mode.

CLRWND

```
subroutine clrwnd
```

Blank the user defined virtual data window without erasing the axes, labels and tic-marks.

SETLAB

```
subroutine setlab(haxlab, vaxlab, tcaptn)
character*80 haxlab, vaxlab, tcaptn
```

Set default plot labels. Must be called before call to window.

Input parameters:

haxlab   label to appear at bottom of graph.

vaxlab   vertical label to appear at left side of graph.

tcaptn   label to appear above graph.

SETPOS

```
subroutine setpos(minx, maxx, miny, maxy)
integer*2 minx, maxx, miny, maxy
```

Define the rectangular screen area on which data is to be plotted in virtual device coordinates. The default is full area of the screen.

Input parameters:

minx   x coordinate of lower-left corner of window

maxx   x coordinate of upper-right corner of window

miny   y coordinate of lower-left corner of window

maxy   y coordinate of upper-right corner of window

SETTIC

```
subroutine settic(xtic, ytic)
integer*2 xtic, ytic
```

Define format for floating point notation tic mark labels. Default format is FORTRAN 1PE10.2.

Input parameters:

xtic   number of decimals horizontal axis tic marks (0 - 3).

ytic   number of decimals on vertical axis tic marks (0 - 3).

SETGRD

```
subroutine setgrd(nxgrd, nygrd)
integer*2 nxgrd, nygrd
```

Set number of grid lines per tic mark. Default = 0.

Input parameters:

nxgrd	number of vertical grid marks per tic.
nygrd	number of horizontal grid mark per tic.

<div align="right">

CONREC

</div>

```
subroutine conrec(d, x, y, z, iub, jub, nc)
integer*4 iub, jub, nc
real*4 d(iub,jub), x(iub), y(jub), z(nc)
```

Plots contours of the function represented by the data points in the array *d*.

Input parameters:

d	2 dimensional array of points representing the function.
x,y	X and Y coordinate arrays.
z	Array of contour levels sorted in ascending order.
iub,jub	Number of data points in the x and y directions.
nc	Number of contour levels.

Bibliography

[1]   W.F. Ames, *Nonlinear Partial Differential Equations in Engineering* (Academic Press, New York, 1965).

[2]   P. Becker and R.J. Field, *J. Phys. Chem.* **89** (1985) 1063.

[3]   M. Brenner, *J. Biol. Chem.* **252** (1977) 4073.

[4]   V. Castets, E. Dulos, J. Boissonade and P. DeKepper, *Phys. Rev. Lett.* **64** (1990) 2953.

[5]   S. Chandrasekhar, *Hydrodynamic and Hydromagnetic Stability* (Oxford, 1961).

[6]   E.J. Doedel, *AUTO: Software for Continuation and Bifurcation Problems in Ordinary Differential Equations* (California Institute of Technology, 1986).

[7]   I. R. Epstein, *Physica D*, in press.

[8]   G.B. Ermentrout, S.P. Hastings and W.C. Troy, *SIAM J. Appl. Math.* **44** (1984) 1133.

[9]   R.J. Field and H.-D. Försterling, *J. Phys. Chem.* **90** (1986) 5400.

[10]   R.J. Field, E. Körös and R.M. Noyes, *J. Amer. Chem. Soc.* **94** (1972) 8649.

[11]   R.J. Field and R.M. Noyes, *J. Chem. Phys.* **60** (1974) 1877.

[12]   R.J. Field and R.M. Noyes, *J. Am. Chem. Soc.* **96** (1974) 2001.

[13]   R.J. Field and R.M. Noyes, *J. Chem. Phys.* **60** (1977) 1877.

[14]   R.J. Field and F.W. Schneider *J. Chem. Ed.* **66** (1989) 195.

[15]   P.C. Fife, *Mathematical Aspects of Reacting and Diffusing Systems*, Lecture Notes in Biomathematics 28 (Springer-Verlag, Berlin, 1979).

[16]   P.C. Fife, J.B. McLeod, *Bull. Amer. Math. Soc.* **81** (1975) 1075.

[17]   P.C. Fife, *J. Chem. Phys.* **64** (1976) 554.

[18]   P.C. Fife, *J. Math. Biol.* **4** (1977) 358.

[19]   R.A. Fisher, *Ann. of Eugenecs* **7** (1937) 355.

[20]   L.K. Forbes, *Physica D* **43** (1990) 140.

[21]   L.K. Forbes, *Physica D* **50** (1991) 42.

[22] C.W. Gear, *Numerical Initial Value Problems in Ordinary Differential Equations* (Prentice-Hall, Englewood Cliffs, NJ, 1971).

[23] J. Górski and A.L. Kawczynski, *Polish J. Chem.* **58** (1984) 847.

[24] J. Górski and A.L. Kawczynski, *Polish J. Chem.* **59** (1985) 61.

[25] A.C. Hindmarsh, *ACM-Signum Newslett.* **15** (1980) 10.

[26] W. Jost, *Diffusion in Solids, Liquids, Gases* (Academic Press, 1960).

[27] Ya.I. Kanel, *Mat. Sborn.* **59** (1962) 243 (in Russian).

[28] A.L. Kawczynski, *Polish J. Chem.* **57** (1983) 1323.

[29] A.L. Kawczynski, *J. Non-Equil. Thermodyn.* **3** (1978) 29.

[30] A.L. Kawczynski, *Polish J. Chem.* in press.

[31] E.F. Keller and L.A. Segal, *J. Theor. Biol.* **26** (1970) 399.

[32] A.N. Kolmogorov, I.G. Petrovskii and N.S. Piskunov, *Bull. Univ. Moscow, Ser Int* **1** (1937) 1.

[33] V.S. Manoranjan and A.R. Mitchell, *J. math. Biol.* **16** (1983) 251.

[34] H. Meinhardt and A. Gierer, *J. Cell Science* **15** (1974) 321.

[35] J.D. Murray, *J. theor. Biol.* **56** (1976) 329.

[36] J.D. Murray, *J. theor. Biol.* **88** (1981) 161.

[37] J.D. Murray, *J. theor. Biol.* **98** (1982) 143.

[38] J.D. Murray, *Mathematical Biology* (Springer-Verlag, Berlin, 1989).

[39] G. Nicolis and I. Prigogine, *Self-Organization in Nonequilibrium Systems* (John Wiley & Sons, New York, 1977).

[40] B. Novak and F.F. Seelig, *J. Theor. Biol.* **56** (1976) 301.

[41] A. Okubo, *Diffusion and Ecological Problems: Mathematical Models* (Springer-Verlag, Berlin, 1980).

[42] M. Orbán, *J. Amer. Chem. Soc.* **102** (1980) 4311.

[43] P. Ortoleva and J. Ross, *J. Chem. Phys.* **63** (1975) 3398.

[44] J.E. Pearson and W. Horsthemke, *J. Chem. Phys.* **90** (1989) 1588.

[45] N. Rashevsky, *Bull. Math. Biophys.* **2** (1940) 15.

[46] J. Rinzel and J.B. Keller, *Biophysics J.* **13** (1973) 1313.

[47] A.B. Rovinsky and A.M. Zhabotinsky, *J. Phys. Chem.* **88** (1984) 6081.

[48] A.B. Rovinsky, *J. Phys. Chem.* **91** (1987) 4606.

[49] A. Saul and K. Showalter In: *Oscillation and Traveling Waves in Chemical Systems*, Editors: R.J. Field and M. Burger (John Wiley & Sons, NY, 1985) 419.

[50] L.A. Segal and J.L. Jackson, *J. Theor. Biol.* **37** (1972) 545.

[51] K. Showalter, *J. Chem. Phys.* **73** (1980) 3735.

[52] J.M. Slack, *Nature* **327** (1987) 553.

[53] C. Thaller and G. Eichele, *Nature* **327** (1987) 625.

[54] A.M. Turing, *Phil. Trans. Roy. Soc.* (London) **B237** (1952) 37.

[55] J.J. Tyson, *J. Math. Biol.* **5** (1978) 351.

[56] J.J. Tyson and P.C. Fife, *J. Chem. Phys.* **73** (1980) 2224.

[57] J.J. Tyson, *J. Chem. Phys.* **86** (1982) 3006.

[58] J.J. Tyson In *Oscillations and Traveling Waves in Chemical Systems*, Editors: R.J. Field and M. Burger (Wiley-Interscience, New York, 1985). p. 93.

[59] J.J. Tyson and J.D. Murray, *Development* **106** (1989) 421.

[60] V.A. Vasiliev, Yu.M. Romanovskii, D.S Chernavskii and V.G. Yakhno, *Autowave Processes in Kinetic Systems* (D. Reidel Publishing Company, Dordrecht, 1987).

[61] J. A. Vastano, J.E. Pearson and W. Horsthemke, *Phys. Rev. Lett.* **124** (1987) 320.

[62] A.T. Winfree, *The Geometry of Biological Time* (Springer-Verlag, 1980).

[63] L. Wolpert, *J. theor. Biol.* **25** (1969) 1.

[64] A.N. Zaikin and A.M. Zhabotinsky, *Nature* **225** (1970) 535.

[65] A. M. Zhabotinskii and A.B. Rovinsky, *J. Phys. Chem.* **94**, 8001 (1990).